

# 1 **Patterns of (trace) metals and microorganisms in the Rainbow hydrothermal vent** 2 **plume at the Mid-Atlantic Ridge**

3 Sabine Haalboom<sup>1,\*</sup>, David M. Price<sup>1,\*,#</sup>, Furu Mienis<sup>1</sup>, Judith D.L van Bleijswijk<sup>1</sup>, Henko C. de  
4 Stigter<sup>1</sup>, Harry J. Witte<sup>1</sup>, Gert-Jan Reichart<sup>1,2</sup>, Gerard C.A. Duineveld<sup>1</sup>

5 <sup>1</sup> NIOZ Royal Netherlands Institute for Sea Research, department of Ocean Systems, and Utrecht University, PO Box 59,  
6 1790 AB Den Burg, Texel, The Netherlands

7 <sup>2</sup> Utrecht University, Faculty of Geosciences, 3584 CD Utrecht, The Netherlands

8 \* These authors contributed equally to this work

9 # Current address: University of Southampton, Waterfront Campus, European Way, Southampton, UK,  
10 SO14 3ZH.

11 [sabine.haalboom@nioz.nl](mailto:sabine.haalboom@nioz.nl); [D.M.Price@soton.ac.uk](mailto:D.M.Price@soton.ac.uk)

12

13 **Keywords:** Rainbow vent; Epsilonproteobacteria; Hydrothermal vent plume; Deep-sea mining; Rare  
14 earth elements; Seafloor massive sulfides

15

## 16 **Abstract**

17 Hydrothermal vent fields found at mid-ocean ridges emit hydrothermal fluids which disperse as neutrally  
18 buoyant plumes. From these fluids seafloor massive sulfides (SMS) deposits are formed which are being  
19 explored as possible new mining sites for (trace) metals and rare earth elements (REE). It has been  
20 suggested that during mining activities large amounts of suspended matter will appear in the water column  
21 due to excavation processes, and due to discharge of mining waste from the surface vessel. Understanding  
22 how hydrothermal plumes can be characterised by means of geochemistry and microbiology as they  
23 spread away from their source and how they affect their surrounding environment may help in  
24 characterising the behaviour of the dilute distal part of chemically enriched mining plumes.

25 This study on the extensive Rainbow hydrothermal plume, observed up to 25 km downstream from the  
26 vent site, enabled us to investigate how microbial communities and (trace) metal composition change in  
27 a natural plume with distance. The (trace) metal and REE content of suspended particulate matter (SPM)  
28 was determined using HR-ICP mass spectrometry and the microbial communities of the neutrally buoyant  
29 plume, above plume-, below plume-, and near-bottom water and sediment were characterised by using  
30 16S rRNA amplicon sequencing methods. Both vertically in the water column and horizontally along the  
31 neutrally buoyant plume, geochemical and biological changes were evident as the neutrally buoyant  
32 plume stood out by its enrichments in (trace) metals and REEs as e.g. Fe, Cu, V, Mn and REE were  
33 enriched by factors of up to ~80, ~90, ~52, ~2.5 and ~40 respectively, compared to above plume water  
34 samples taken at 1000 m water depth. The concentrations of these elements changed as the plume aged  
35 shown by the decrease of element/Fe molar ratios of chalcophile elements (Cu, Co, Zn), indicative of  
36 rapid removal from the hydrothermal plume or removal from the solid phase. Conversely, increasing  
37 REE/Fe molar ratios imply uptake of REE from the ambient seawater onto Fe-oxyhydroxides. This was  
38 also reflected in the background pelagic system as Epsilonproteobacteria started to dominate and  
39 univariate microbial biodiversity declined with distance away from the Rainbow hydrothermal vent field.  
40 The Rainbow hydrothermal plume provides a geochemically enriched natural environment, which is a  
41 heterogeneous, dynamic habitat that is conducive to ecological changes in a short time span. This study  
42 of a hydrothermal plume provides a baseline study to characterize the natural plume before the  
43 interference of deep-sea mining.

44

## 45 **1 Introduction**

46 Hydrothermal vent fields found at mid-ocean ridges and back-arc basins are known for discharging fluids  
47 rich in potential microbial energy sources such as H<sub>2</sub>, H<sub>2</sub>S, CH<sub>4</sub>, NH<sub>4</sub> and Fe (Jannasch and Mottl, 1985;  
48 McCollom, 2000). In addition, they are characterised by the presence of polymetallic sulfide deposits  
49 containing high grades of metals like Cu, Co, Zn and rare earth elements (REE) (Cave et al., 2002;  
50 Chavagnac et al., 2005). Because of the steadily increasing demand for these metals, and their geo-  
51 political distribution on land, hydrothermal vent deposits are explored as new mining sites (Hoagland,

52 2010). Since such areas accommodate unique and vulnerable marine life, serious concerns exist about the  
53 environmental sustainability of seafloor massive sulfide (SMS) deposit mining (Boschen et al., 2013;  
54 Collins et al., 2013), especially with regards to the effects of the different plumes, which are generated  
55 during the excavation of ores and by the return flow of wastes in the vicinity of hydrothermal vents  
56 (Ramirez-Llodra et al., 2011; Vare et al., 2018). As SMS mining will concentrate on deposits around  
57 hydrothermal vents, and not on active vents or chimneys due to technical risks associated with high  
58 temperatures (Gwyther et al., 2008), it is likely that the background and extinct vent communities (from  
59 microorganisms to megafauna) will be impacted through habitat loss, mechanical destruction, noise,  
60 smothering and bioaccumulation of toxic substances (Levin et al., 2016). However, knowledge about the  
61 background ecosystem and natural plume is sparse, as the vents and their proximal fauna have attracted  
62 most of the attention, for example in microbiology (e.g. Han et al., 2018; Cerqueira et al., 2018).

63 To fill this gap, the Dutch TREASURE project (STW-NWO) was focussed on describing the structure of  
64 the background pelagic and benthic communities of an active hydrothermal vent site with SMS deposits  
65 on the Mid-Atlantic Ridge (MAR). The Rainbow hydrothermal vent (36°14' N on the MAR) was selected  
66 for this study as it ejects one of the most prominent and persistent natural plumes on the MAR.  
67 Hydrothermal plumes represent a distinct natural ecosystem in itself, which under the influence of  
68 currents may extend tens of kilometres away from its point of origin. Basic knowledge of natural plumes  
69 is essential to be able to discern impacts arising from future SMS mining plumes created in the vicinity  
70 of the hydrothermal vent which are likely interfere with the natural hydrothermal plume. Though mining  
71 plumes will have a higher initial density and therefore tend to sink rather than maintain buoyancy  
72 (Gwyther et al., 2008; Boschen et al., 2013), the finest and slowest sinking fraction of suspended solids  
73 in the mining plume may interfere with the natural plume during its dispersal, especially when released  
74 above the seafloor.

75 Since the discovery of the Rainbow hydrothermal vent field in 1996 by German et al., several studies  
76 concerning the composition of the hydrothermal fluid and the sediment influenced by fall-out of  
77 particulates from the Rainbow and other hydrothermal plumes have been published. These showed, for  
78 example, that the underlying host rock influences the hydrothermal fluid composition (Wetzel and Shock,

79 2000; Marques et al., 2006). Geochemical investigation of sediment by Cave et al. (2002) at distances of  
80 2 to 25 km from the Rainbow hydrothermal vent field showed enrichments of Fe, Cu, Mn, V, As and P,  
81 as well as REE (Chavagnac et al., 2005) as a result of fallout from the hydrothermal plume. It has further  
82 been shown that microbial activity influences geochemical processes in the plume (Breier et al., 2012;  
83 Dick et al., 2013), such as scavenging and oxidation of metals (Cowen and Bruland, 1985; Cowen et al.,  
84 1990; Mandernack and Tebo, 1993; Dick et al., 2009), influencing the local ocean geochemistry.

85 Microbial activity within the plume is fuelled by redox reactions that provide energy for  
86 chemolithoautotrophic microbial taxa. The abundance of energy sources within plumes support a plethora  
87 of chemolithoautotrophic microbial communities (e.g. Orcutt et al., 2011; Frank et al., 2013;  
88 Anantharaman et al., 2016). Plume microbial communities can be distinct or relatively similar to  
89 background communities (Dick and Tebo et al., 2010; Sheik et al., 2015; Olins et al., 2017), with plume  
90 associated bacteria originating from either seafloor communities, background seawater communities or  
91 from growth within the plume (Dick et al., 2013). Djurhuus et al. (2017) observed the reduction in  
92 dominance of vent associated microorganisms with increased redox potential, suggesting that  
93 communities associated with the initial rising plume become diluted on a scale of metres. Comparatively  
94 little is known about changes in chemical composition and microbial assemblages in the hydrothermal  
95 plume after its initial rise, when it becomes neutrally buoyant and is dispersed by currents, remaining  
96 traceable in particulate form to at least 50 km away from its source (Severmann et al., 2004), and even up  
97 to 4000 km in dissolved form (Resing et al., 2015). Considering the majority of microbial growth is  
98 predicted to occur in the neutrally buoyant portion of the plume (Reed et al., 2015), further efforts should  
99 be concentrated on sampling this portion of the plume.

100 In order to address this gap, water column and sediment samples from the Rainbow hydrothermal vent  
101 area were investigated during the TREASURE cruise. Geochemical and biological changes were explored  
102 vertically in the water column and horizontally along the neutrally buoyant plume using HR-ICP mass  
103 spectrometry to determine the (trace) metal and REE content of the SPM. Next generation sequencing  
104 methods were used to quantify the microbial diversity in the pelagic system that was influenced by the  
105 hydrothermal plume. Whilst mechanistic understanding of microbial and geochemical interactions in the

106 plume would have required a different experimental setup, which was beyond the scope of the  
107 TREASURE project, this paper aims to contribute to knowledge of geochemical and biological  
108 heterogeneity in the surroundings of an SMS site, induced by the presence of an active hydrothermal  
109 plume, which should be taken into account in environmental impact assessments of SMS mining.

110

## 111 **2 Material and methods**

### 112 **2.1 Study site**

113 The Rainbow hydrothermal vent field (Fig. 1) is located on the Mid Atlantic Ridge (MAR) at 36°13.80  
114 N, 33°54.14 W at approximately 2300 m water depth, southwest of the Azores. The vent field is located  
115 on the western flank on the non-volcanic Rainbow Ridge, in an offset between the South Alvin Mid  
116 Atlantic Ridge (AMAR) and AMAR segments of the MAR (German et al., 1996; Fouquet et al., 1998;  
117 Douville et al., 2002). It is located at the intersection between the non-transform fault system and the  
118 ridge faults (Charlou et al., 2002), making this vent field tectonically controlled. The vent field, which is  
119 approximately 100 by 250 m in size, is underlain by a basement composed of ultramafic rocks (Edmonds  
120 and German, 2004; Marques et al., 2006). The ultramafic setting of Rainbow is atypical for the region,  
121 which is dominated by basalt hosted vent systems (Douville et al., 2002). Due to serpentinization reactions  
122 during the circulation of the hydrothermal fluid in the peridotite basement rocks, the Rainbow vent field  
123 produced plumes particularly enriched in transition metals (notably Fe, Mn and Cu) and REE (Douville  
124 et al., 2002; Findlay et al., 2015). On the contrary the plumes are depleted in hydrogen sulfides (Charlou  
125 et al., 2002; Douville et al., 2002), resulting in relatively high metal/sulfide ratios. Consequently, the  
126 chimneys and the SMS deposits of the Rainbow hydrothermal field are enriched in Cu, Zn, Co and Ni  
127 when compared to vent systems with a basaltic host rock (Charlou et al., 2002).

128 The vent field consists of 10 active, high temperature (365 °C) black smokers and emits an extensive  
129 plume with a distinct chemical composition compared to the ambient seawater (Severmann et al., 2004).  
130 The plume is considered the largest and widest spreading in the region (German et al., 1996), rising up to  
131 200 m above its source and was traceable over at least 50 kilometres (Severmann et al., 2004). Controlled

132 by the local hydrodynamic regime and topography (Thurnherr and Richards, 2001; Thurnherr et al.,  
133 2002), the neutrally buoyant plume moves predominantly to the north and east around the Rainbow Ridge  
134 with an average current speed of 5-6 cm s<sup>-1</sup> and continues in a northward direction along the southern and  
135 eastern side of the rift valley of the AMAR segments (Edmonds and German, 2004). Characteristics and  
136 behaviour of the Rainbow plume are relatively well-studied which make the Rainbow vent field a suitable  
137 site to study neutrally buoyant plumes.

138

## 139 **2.2 Water column and sediment sampling**

140 Water samples and sediment cores were collected along the path of the plume during RV *Pelagia* cruise  
141 64PE398 in April 2015. Five putatively distinct biotopes were sampled: (i) above plume (1000 m water  
142 depth), (ii) plume, (iii) below plume (10 metres above bottom), (iv) near-bottom water and (v) sediment.

143 Using CTD casts with a Seabird 911 CTD-Rosette system, the plume was traced in real time using  
144 turbidity as an indicator, measured in NTU with a WETLabs turbidity sensor. Other variables measured  
145 included temperature (°C), salinity (PSU), density ( $\sigma\text{-}\theta$ , kg m<sup>-3</sup>), dissolved oxygen (ml L<sup>-1</sup>) and  
146 chlorophyll ( $\mu\text{g L}^{-1}$ ). At five stations, continuous yoyo CTD-casts were taken over the course of 12 hours,  
147 to study the temporal changes of the hydrothermal plume.

148 A total of 41 water samples were collected using 12 L Niskin bottles from eleven downstream stations,  
149 two distal downstream stations and three upstream stations. Once the CTD was back on deck, three  
150 distinct water samples were immediately taken for suspended particulate matter (SPM), trace metals, and  
151 the microbial community.

152 Depths for sampling SPM were chosen to comprise the largest variation in turbidity measured by the  
153 WETLabs turbidity sensor in a vertical profile so that the sensor could be reliably calibrated and readings  
154 converted to mg L<sup>-1</sup>. If possible, trace metal and microbial community samples were taken at the same  
155 stations and/or same depth.

156 Sediment and near-bottom water samples were collected with a NIOZ designed box corer of 50 cm  
157 diameter equipped with a top valve to prevent flushing, subsequently trapping near-bottom water (van  
158 Bleijswijk et al., 2015). In total eight cores were collected (Table 1). Due to unsuitable coring substrates,  
159 CTD locations and coring sites did not always follow the same track. Box cores were taken on the eastern  
160 part of the Rainbow Ridge, continuing in the basin east of the ridge, while two cores were taken on the  
161 north-western flank of the ridge, following the path of the plume.

162

### 163 **2.3 Suspended particulate matter analysis**

164 From each 12 L Niskin bottle, two 5 L subsamples were collected to determine the concentration of SPM.  
165 The subsamples were filtered on board over pre-weighed 0.4  $\mu\text{m}$  polycarbonate filters. The filters were  
166 rinsed with  $\sim 10$  ml of Milli-Q water to remove salt, while still applying under pressure, and subsequently  
167 stored at  $-20$   $^{\circ}\text{C}$  on board. In the laboratory, the filters were freeze dried and then weighed in duplo, or in  
168 triplo if the difference between the first two measurements was more than 0.03 mg. To yield SPM  
169 concentrations, the net dry weight of the SPM collected on the filters (average of 0.25 mg), corrected by  
170 the average weight change of all blank filters (0.04 mg), was divided by the volume of filtered seawater  
171 (5 L). Subsequently, the filters were examined using a Hitachi TM3000 table-top scanning electron  
172 microscope (SEM) connected to an energy-dispersive spectroscopy (EDS)-detector to visualize content  
173 of the SPM and to qualitatively analyse the chemical composition. The SEM was operated under an  
174 acceleration voltage of 15 kV and a filament current of 1850 mA.

175

### 176 **2.4 Chemical analysis**

177 For analysis of major and trace metals present in particulate form in and around the hydrothermal plume,  
178 water samples were filtered on board over acid-cleaned 0.45  $\mu\text{m}$  polysulfone filters directly from the  
179 Niskin bottle at ambient temperature while applying under pressure. A water barrel in between the  
180 filtration holder and pump allowed for volume measurements of water filtered. The filters were  
181 subsequently stored at  $-20$   $^{\circ}\text{C}$  until further examination. Filters were dried in the laboratory in an Interflow

182 laminar flow bench at room temperature prior to analysis. Subsequently, the filters were placed in acid-  
183 cleaned Teflon vials and were subjected to a total digestion method. For this purpose a mixture of 6.5 ml  
184 HNO<sub>3</sub> (ultrapure)/HF (suprapure) (10:1) solution, 1 ml HCl (ultrapure) and 1 ml HClO<sub>4</sub> (ultrapure) was  
185 added to the vials, after which the vials were covered and placed in an Analab hotblock for 48 hours at  
186 125 °C. After the filters were completely dissolved, the covers were taken off from the vials and the vials  
187 were left for 24 hours in order to evaporate the acids. Finally, the residue was taken up again in 10 ml 1M  
188 ultra grade HNO<sub>3</sub>, pre-spiked with 5 ppb scandium and 5 ppb rhodium as internal standards. Furthermore,  
189 ten procedural blanks were performed. Half of them were empty acid-cleaned Teflon vials, the other five  
190 contained an acid-cleaned blank filter in order to correct for the dissolved filters. These blanks were  
191 subjected to the same total digestion method as described above. A HR-ICP-MS (Thermo Element II) at  
192 the Royal Netherlands Institute for Sea Research (NIOZ) was used to analyse the concentrations of major-  
193 and trace metals, as well as REEs. The concentrations were calculated using external calibration lines  
194 made from a multi stock solution, which was prepared by mixing Fluka TraceCert standards for ICP. Rh  
195 was used as an internal standard for all elements. The machine drift was measured before, half-way and  
196 after each series of samples and was monitored by using an external drift solution. Precision (relative  
197 standard deviation (RSD)) of these analyses was generally <2 % for major- and trace metals, apart from  
198 <sup>115</sup>In where the RSD values generally are between 4 % and 8 %, with maximum values going up to 12.48  
199 %. For REE, the RSD values were generally <3 %, apart from a few measurements where RSD values  
200 reached maximums up to 12.48 %. The accuracy could not be determined as no certified reference  
201 material was analysed. The data of the samples was corrected for the dissolved filters by subtracting the  
202 average result of the five blank filters. Subsequently the data was recalculated to account for the dilution  
203 of the samples during the total digestion and the amount of seawater that was filtered to yield the true  
204 concentration of each element.

205

## 206 **2.5 Microbial community**

207 Three distinct samples of 2 L of water were collected from three different Niskin bottles for Next  
208 Generation Sequencing (NGS). The water was filtered immediately after collection through a 0.2 µm

209 polycarbonate filter (Nuclepore) facilitated by a vacuum of 0.2 bar, in a climate controlled room at 4 °C  
210 to limit DNA degradation. From the box cores >0.25 grams of surface sediment were scraped off with a  
211 sterilised spatula, whilst 1.5 litre of overlying (near-bottom) water was filtered as above. Filters were  
212 stored in a 2 ml cryo-vial and all samples were stored at -80 °C on board.

213 DNA was extracted using a Power Soil DNA Isolation Kit (MoBio, now Qiagen) according to the  
214 manufacturer's protocol. Each DNA extract concentration was quantified using a Qubit 3.0 fluorimeter  
215 (Qiagen, Inc.) and stored at -20 °C before amplification. Extracts were combined with Phusion Taq  
216 (Thermo Scientific), High Fidelity Phusion polymerase buffer and universal primers to amplify the V4  
217 region of 16 S rDNA of bacteria and archaea (Table 2), with unique molecular identifier (MID)  
218 combinations to identify the different samples. All negative controls from all PCR series were labelled  
219 with the same unique MID. The PCR settings were as follows: 30s at 98 °C, 29 cycles (10s at 98 °C, 20s  
220 at 53 °C, 30s at 72 °C) and 7 minutes at 72 °C. Four and three samples were re-run at 30 and 32 cycles,  
221 respectively, in order to yield enough product. Each sample was subjected to the polymerase chain  
222 reaction (PCR) protocol in triplicate and processed independently to avoid bias. 5 µl of product was used  
223 to screen the products on an agarose gel. The remaining 25 µl of each triplicate was pooled to evenly  
224 distribute the DNA, split into two slots and run on a 2 % agarose gel at 75 volts for 50 minutes. Sybergold  
225 stain was applied post run for 20-30 minutes before cutting the 380 bp bands out with a sterilised scalpel  
226 over a blue light to avoid UV damage. The two bands of mixed triplicates were pooled, purified using the  
227 Qiaquick Gel Extraction Kit (Qiagen, Inc.) and quantified with a Qubit™ 3.0 fluorometer (Qiagen, Inc.).  
228 Samples were pooled in equimolar quantities together with blank PCR controls. The pooled sample was  
229 concentrated using MinElute™ PCR Purification columns (Qiagen Inc.) as described by the manufacturer  
230 and sent to Macrogen (South Korea) for sequencing. Sequencing was undertaken with a Roche GS FLX  
231 instrument using Titanium chemistry on a one-eight region gasket and Roche GS FLX instruments.  
232 Sequence processing was undertaken as described by van Bleijswijk et al. (2015), using a QIIME pipeline.  
233 Sequences shorter than 250 bases and average Q scores below 25 were removed. The OTU sequences  
234 (>98 % similarity) were classified (>93 % similarity) based on a recent SILVA SSU database (release  
235 132; Yilmaz et al. 2014). Single reads were excluded and all data were standardised to remove any  
236 disproportionate sampling bias.

237

## 238 **2.6 Statistics**

239 Unconstrained ordination techniques were utilised to distinguish biotopes and general community  
240 patterns. Non-metric Multi-Dimensional Scaling plots (NMDS) were created based upon Bray-Curtis  
241 similarity matrices of square root transformed microbial community assemblages. Group average  
242 clustering was also utilised in order to quantify similarities between the samples. ANalysis Of SIMilarities  
243 (ANOSIM) was subsequently used to statistically test community distinctions based upon presumed  
244 biotopes (sediment, near-bottom water, below plume water, plume water and above plume water). In  
245 addition, all water column samples were plotted in separate NMDS plots to observe patterns in greater  
246 detail. Physical properties of all water samples (station, depth, turbidity and location) were depicted in a  
247 NMDS plot to observe sample similarities. These environmental data were normalised and Euclidean  
248 distance was used to create a similarity matrix. The relationship between Fe and turbidity was tested with  
249 a linear regression analysis. Trace metals and REE were normalised to Fe, since it is the primary particle-  
250 forming element at all stages of plume dispersion, giving insight in the chemical behaviour. All  
251 multivariate statistics were undertaken in Primer™ V6 (Clarke and Gorley, 2006).

252 Shannon-Wiener index ( $\log e$ ) was calculated as a diversity measure. Biodiversity differences between  
253 biotopes were tested with the non-parametric test Kruskal-Wallis with pairwise comparisons as the data  
254 did not meet normality or homogeneity assumptions, even after transformation. These statistical tests  
255 were undertaken in SPSS.

256 A SIMilarities PERcentage analysis (SIMPER in Primer v6) was applied on the microbial class level  
257 with a cut off for low contributions at 90 % based on Bray-Curtis similarity matrix to characterise the  
258 community composition based on groups contributing to intra biotope similarities. Relationships between  
259 environmental variables and microbial classes as a percentage of each composition within the plume,  
260 were tested with Pearson correlation and hierarchical clustering to identify broad response groups.

261

## 262 **3 Results**

### 263 **3.1 Water column characteristics**

264 Temperature, salinity and density plots indicated that the water column at each location had similar  
265 physical traits, whereby three main different water masses could be distinguished (Supplement Fig. S1).  
266 The surface Eastern North Atlantic Central Water (ENACW) was characterised by a temperature, salinity  
267 and density at the surface of 18 °C, 36.4 PSU and 26.2 kg m<sup>-3</sup> to 11 °C, 35.5 PSU and 27.2 kg m<sup>-3</sup> at the  
268 bottom of the water mass. The underlying Mediterranean Outflow Water (MOW) was characterised by a  
269 temperature of 7.5-11 °C, a salinity of 35.4-35.5 PSU and a density of 27.2-27.75 kg m<sup>-3</sup>. The North  
270 Atlantic Deep Water (NADW) was characterised by temperatures ranging from 4 to 7.5 °C, salinity of  
271 35.0 to 35.4 PSU and a density of 27.75 to 27.825 kg m<sup>-3</sup> (Emery and Meincke, 1986). The neutrally  
272 buoyant plume was centred around the 27.82 kg m<sup>-3</sup> isopycnal, as illustrated in Figures 2 and 3.

273

### 274 **3.2 Turbidity and plume dispersion**

275 Against a background of non-plume influenced waters, as found in the CTD casts, with typical  
276 concentrations of SPM of 0.04 mg L<sup>-1</sup> (0.015 NTU), the neutrally buoyant plume stands out as a layer  
277 with distinctly higher turbidity values (i.e. higher SPM concentrations) consistently present in the depth  
278 interval of 1750 – 2400 m at stations located north and east of Rainbow (Fig. 2). Except where this turbid  
279 water layer was found impinging the seabed, relatively clear waters separated the turbid layer from the  
280 underlying seabed.

281 At downstream stations, a consistent trend of decreasing turbidity and increasing vertical dispersion was  
282 noted. At station 27, 3.5 km north of Rainbow, maximum turbidity in the core of the plume was 0.15 NTU  
283 (0.09 mg L<sup>-1</sup>) and plume thickness was about 105 m, whilst at station 46, 15.2 km east of Rainbow,  
284 maximum turbidity was only 0.08 NTU (0.06 mg L<sup>-1</sup>) and plume thickness was 275 m. Away from the  
285 main plume path, station 47 and 49 (13.8 and 16.5 km from Rainbow, respectively) showed a diluted  
286 signature similar to that observed at the most distal stations along the main plume path. Despite being  
287 most proximal to Rainbow, station 16, located 1.0 km downstream of Rainbow, showed a relative low  
288 turbidity of 0.015 NTU (0.04 mg L<sup>-1</sup>). Since the plume is more constrained closer to the source, the main

289 body of the narrower plume could have been missed with the CTD. Stations upstream of the vent site  
290 (station 13 and 28, 4.2 and 7.5 km southwest of Rainbow respectively and station 40, 3.6 southeast of  
291 Rainbow) displayed low turbidity values, ranging between 0.01 and 0.02 NTU ( $0.04 \text{ mg L}^{-1}$ ) (Fig. S2).

292 The CTD profiles from stations 42 and 49 (4.9 and 16.5 km north of Rainbow respectively) both displayed  
293 highest turbidity in the lower hundreds of metres above the seafloor, with instances of seafloor contact  
294 during time of sampling. Therefore no samples could be taken below the plume at these stations. The  
295 assumption that the plume is subject to vertical movement is supported by observations made during 12-  
296 hour CTD yoyo casts carried out at station 27 (Fig. 3). Along with vertical displacements of the  $27.82 \text{ kg}$   
297  $\text{m}^{-3}$  isopycnal on the order of 150 m, likely reflecting internal tidal motions, the hydrothermal plume was  
298 found to also move up and down, at times touching the seafloor.

299

### 300 **3.3 Enrichment of (trace) metals compared to the ambient seawater**

301 NMDS ordination (Fig. 4) based on Euclidean distance resemblance of normalised element/Fe molar ratio  
302 data of all collected water samples (2D stress = 0.03), revealed a clear distinction of the different samples.  
303 Most outstanding are the samples from above plume waters, indicating that the chemical composition is  
304 different from the other samples.

305 The remaining samples showed less variation, nonetheless the samples collected from below the plume  
306 and the samples collected away from the main path of the plume can be distinguished. This shows that  
307 the hydrothermal plume can be characterised by its chemical composition. When comparing samples  
308 taken in the turbidity maximum of the plume to the above plume water samples taken at 1000 m water  
309 depth it is found that Fe, Cu, P, V and Pb are enriched by factors of ~80, ~90, ~17, ~52 and ~25  
310 respectively. Elements with a more moderate degree of enrichment are Co, Mn, Zn, Al and Ni, with  
311 enrichment factors of ~8.0, ~2.5, ~10.3, ~1.4 and ~1.6, respectively. The REEs were enriched by a factor  
312 of 5 to 40 relative to the clear water. U, Ti and Ca are slightly enriched at turbidity maxima, by factors of  
313 ~1.3, ~1.6 and ~1.2, respectively. In and Sn are depleted compared to the above plume water.

314

### 315 3.4 Geochemical gradients within the hydrothermal plume

316 Within the hydrothermal plume, geochemical evolution is found as the plume disperses. Visual  
317 examination of the samples with the SEM coupled with chemical analysis performed with the EDS-  
318 detector revealed that the SPM within the plume close to the Rainbow hydrothermal vent at station 32  
319 (2.9 km north of Rainbow) mainly consisted of Fe-sulfides. In the plume samples further downstream, Fe  
320 is mainly present as Fe-oxides, Fe-hydroxides or bound in alumino-silicates.

321 Chemical examination of the samples showed gradients in the element/Fe molar ratios along the path of  
322 the plume as well as off the main path of the plume at upstream and the most distal downstream stations.  
323 Since the Fe concentration is linearly related to the turbidity (Fig. 5) ( $R^2 = 0.9356$ ,  $P < 2.2 \cdot 10^{-16}$ ),  
324 normalisation to Fe reveals relative enrichments or depletion of common elements. The chalcophile  
325 elements Co, Cu and Zn show a partly-linear relation steepening with increasing Fe concentration (Fig.  
326 6A for Cu), indicating that the element/Fe molar ratios are elevated close to the source but decrease  
327 towards the more distal sites (Fig. 7A). One exception is the Zn/Fe molar ratio, which is elevated at station  
328 37, 39 and 44. Furthermore, a high Zn/Fe molar ratio is observed at upstream station 40. The oxyanions  
329 P and V are linearly related to Fe (Fig. 6B for V), and shows varying element/Fe molar ratios without a  
330 clear trend of increasing or decreasing ratios, both upstream and downstream of Rainbow (Fig. 7B). The  
331 REE show a partly-linear relation levelling-off with increasing iron concentrations (Fig. 6C for Y). Within  
332 the plume this is displayed as increasing element/Fe molar ratios towards station 44, with station 42 as an  
333 exception, followed by slightly decreasing molar ratios from station 44 onwards (Fig. 7C). The Ca/Fe  
334 molar ratios ranged between 0 and 15 for most of the downstream stations, apart from the stations further  
335 downstream (47 and 49), which displayed slightly higher Ca/Fe molar ratios. Upstream station 28 had a  
336 Ca/Fe molar ratio similar to those found at station 47 and 49 and upstream station 40 was found to have  
337 a significantly higher Ca/Fe molar ratio (Fig. 7E). Other analysed elements, Mn, Al, Ni, In, Pb, Sn, Ti  
338 and U showed no clear relationship with the Fe concentration (Fig. 6D for Sn). However, within the plume  
339 it was found that the Mn/Fe molar ratio is lower than at the upstream stations or the more distal  
340 downstream stations.

341

### 342 **3.5 Microbial assemblages in water column biotopes**

343 Samples from sediment, near-bottom water and no plume water contained microbial communities which  
344 clustered distinctly from each other and from plume, below-plume and above-plume communities (Fig.  
345 8). In particular, sediment, near-bottom water and no-plume (station 13) samples have communities that  
346 are very dissimilar from the overlying water column samples. Sediment samples appeared to cluster in a  
347 straight line suggesting some sort of gradient of similarity along the ordination axis, though no apparent  
348 patterns were observed when independently plotted. The near-bottom water samples were relatively  
349 dispersed in the NMDS plot suggesting a more variable community. Samples taken at the upstream station  
350 13 from below-plume and plume depths showed no similarity with samples from corresponding depths  
351 in the other stations, whilst the above-plume community at this station is consistent with that of other  
352 stations. In general, plume and below-plume communities were more similar nearer to the vent source,  
353 with stations further downstream displaying greater dissimilarity (Fig. 9, Fig. S3).

354 Group average cluster analysis showed high level of dissimilarity, i.e. large community variation, between  
355 and within biotopes. ANOSIM revealed all putative biotopes that were sampled had distinct communities  
356 (Global R = 0.738; p = 0.001; 999 permutations), except for plume and below plume samples which could  
357 not be distinguished statistically (Global R = -0.091; P = 0.861). The two seemingly unique samples from  
358 station 13 also tested significantly distinct, but with a low number of permutations (<999) due to low  
359 replication (n=2).

360

### 361 **3.6 Univariate biodiversity**

362 Plume and below plume samples were less diverse than sediment samples, whilst diversity in the plume  
363 was lower than in near-bottom water samples (Kruskal-Wallis:  $\chi^2(4) = 36.127$ ,  $P < 0.01$ ). In general,  
364 plume diversity was low (Fig. 10), but further differences were not statistically significant, likely due to  
365 limited replication and intra biotope variation.

366 The plume microbial community at sites upstream of Rainbow and at the immediate downstream sites  
367 (stations 28, 16 and 27) showed similar and relatively high biodiversity ( $>4.5$ ) (Fig 11). Plume

368 biodiversity at the sites further away from Rainbow gradually decreased until station 46, which displayed  
369 the lowest Shannon-Wiener index value of 2.4. Distant stations 47 and 49, showed biodiversity rising to  
370 a more moderate index value around 3.5.

371

### 372 **3.7 Species composition**

373 Results of the SIMPER analyses showing the contributions of taxa composition to similarities within  
374 biotopes (Table 3), mirrored the NMDS and ANOSIM results whereby the similarity of community  
375 composition in each biotope was dominated by a different makeup of the microbial community. The  
376 Archaeal class Nitrososphaeria (Marine group 1 archaea) contributed the most to similarity within the  
377 above and below plume water communities, while also being very common in all water samples.  
378 Alphaproteobacteria, Gammaproteobacteria and Deltaproteobacteria also constituted as a large makeup  
379 of all biotopes in the area. The class Epsilonproteobacteria were largely absent from above plume samples  
380 being not influenced by the plume, and only contributed <2 % to near-bottom water communities. By  
381 contrast, Epsilonproteobacteria were dominant in plume water samples (accounting for >35 % of the  
382 community), and were the fifth most dominant taxon in below plume water samples contributing 8.9 %  
383 of the community.

384 Epsilonproteobacteria accounted for about 20 % of the plume community at stations near the vent. Beyond  
385 the near vent stations, an increase in relative abundance of Epsilonproteobacteria with distance from vent  
386 was observed, accounting for 64 % of the community at the distant station 46 (Fig. 12).  
387 Alphaproteobacteria, Deltaproteobacteria and Gammaproteobacteria appeared to become less dominant  
388 with distance from the plume source (Fig. 12). The communities at distant stations 47 and 49 were less  
389 dominated by Epsilonproteobacteria (around 40 %). Below plume communities were dominated mostly  
390 by Nitrososphaeria (Marine group 1 Archaea) whereby Nitrosphaeria became more dominant with  
391 distance from the plume source likewise as the Epsilonproteobacteria in the plume. Correlations between  
392 environmental variables (elemental chemistry and physical properties) and all microbial classes observed  
393 in the plume were evident and appeared class specific (Fig. S4). The hierarchical clustering revealed eight  
394 broad response groups, which displayed different relationships with the environmental variables.

## 395 **4 Discussion**

396 Using a multidisciplinary approach in which physical, geochemical and ecological data were collected  
397 from the Rainbow vent neutrally buoyant plume and its underlying sediment, we aimed to expand  
398 knowledge and characteristics of the background (i.e. before impact) state of a hydrothermal vent. Such  
399 knowledge is deemed essential to be able to assess (potential) impacts of future deep-sea SMS mining, as  
400 it may help in characterising the behaviour of the dilute distal part of chemically enriched mining plumes.  
401 We found geochemical and microbial differences between the above-plume, plume, below plume and no-  
402 plume water and in addition, pertinent chemical and biological gradients within the extensive Rainbow  
403 hydrothermal vent plume were evident.

404

### 405 **4.1 Physical constraints of plume location and behaviour**

406 The plume was observed within the NADW mass, constrained to an isopycnal density envelope of 27.82  
407  $\text{kg m}^{-3}$  (Fig. 2 and 3). The apparent continuity of this turbid water layer, especially to the NE of the  
408 Rainbow field, and lack of similarly turbid waters in the bottom waters below the plume, link the plume  
409 to Rainbow and preclude local sediment resuspension as origin. Using turbidity measurements and  
410 presumed plume path, we traced the plume up to 25 km away from the vent source. This is within the  
411 range mentioned by German et al. (1998) who found that the Rainbow plume extends over 50 km, being  
412 controlled by local hydrodynamics and topography. Unexpectedly, in the basin upstream of the Rainbow  
413 vent field a turbidity peak at 1975 m water depth resembling a plume was observed as well (station 28),  
414 confounding our assumption of a clear water column at upstream stations and distant downstream stations.  
415 This suggests that the plume is distributed much further than previously observed by Thurnherr and  
416 Richards (2001) and German et al. (1998). This is exemplified by the local variation in microbial  
417 community composition of upstream stations (Fig. 12) and is supported by the relatively low Ca/Fe molar  
418 ratio at station 28 (Fig. 7), indicating hydrothermal influence. In addition, the observed variability of  
419 plume strength and vertical position (Fig. 3) indicate that local fluctuation in the current regime and tidal  
420 motions influence the plumes behaviour. This dynamic behaviour has implications for surveys designs  
421 and should be considered when monitoring natural and man-made plumes, such as mining-related plumes.

422 Prior insight into plume extension and behaviour is required for the identification of adequate control sites  
423 and for tracking of plume evolution in future impact studies.

424

## 425 **4.2 Plumes influence on the water column chemical and microbial make-up**

426 The neutrally buoyant plume introduced pelagic heterogeneity in terms of chemical and microbial  
427 composition, which is supported by the vertical classification of the different biotopes. The neutrally  
428 buoyant plume was evidently enriched in metals and REE compared to overlying clear water. Element  
429 concentrations were found to be in line with those found by German et al. (1991) and Edmonds and  
430 German (2004) who have studied the Trans-Atlantic Geotraverse (TAG) hydrothermal plume and the  
431 Rainbow hydrothermal plume, respectively. Our chemical results from Rainbow also match with those of  
432 Ludford et al. (1996), who have studied vent fluid samples from the TAG, Mid-Atlantic Ridge at Kane  
433 (MARK), Lucky Strike and Broken Spur vent sites, i.e. element concentrations were found to be in the  
434 same order of magnitude (Table S2).

435 The distinctive chemical composition of the plume samples (e.g. metal concentrations) affects  
436 chemolithoautotrophic microbial growth within the plume as indicated by the typical microbial  
437 community in plume samples. Unlike Sheik et al. (2015), we observed a clear and consistent separation  
438 between communities in the plume and those in above-plume samples. The influence of MOW on the  
439 above-plume community could also play a role, as water masses can harbour different microbial  
440 communities (Agogue et al., 2011). However, the palpable presence of a plume in the turbidity data with  
441 supporting chemical measurements, and the occurrence of vent associated Epsilonproteobacteria (Olins  
442 et al., 2017; Djurhuus et al., 2017) and other vent associated groups such as the Gammaproteobacteria  
443 clade SUP05 (Sunamura et al., 2004), point to a unique chemical environment. Here chemosynthetic  
444 communities flourish and give rise to independent biotopes in the neutrally buoyant plume kilometres  
445 downstream of the vent site.

446 Below-plume communities were not distinct from the plume biotope, although instead of  
447 Epsilonproteobacteria, the ubiquitous class Nitrososphaeria was the most dominant group, reflecting

448 some similarities with above-plume seawater communities. Similarities between plume and proximal  
449 habitat communities have also been observed by Olins et al. (2017), whereby intra-field (defined as within  
450 vent field between diffuse flows) and diffuse flow microbial communities were alike. In our study,  
451 similarities between plume and below-plume are likely derived by precipitation of mineral and microbial  
452 aggregates dragging plume microbes deeper below the plume as suggested by Dick et al. (2013). In  
453 addition, internal wave induced turbulence causes vertical mixing along the slope of the Rainbow Ridge  
454 (van Haren et al., 2017), which may cause the plume and associated communities near the vent field to  
455 mix with ambient water communities leading to assemblage similarities. This indicates the plume and  
456 associated microbial processes could have a larger vertical footprint than previously observed, supporting  
457 suggestions by Olins et al., (2017) that proximal non-plume habitats have been overlooked. Interestingly,  
458 near-bottom water (and sediment) community assemblages were distinct from the below-plume and other  
459 water column communities. This could imply: 1) that there is little "fall out" from the plume at distance  
460 from the vent which is in agreement with sediment trap observations by Khripounoff et al. (2001), 2)  
461 plume specific bacteria die off due to lack of energy sources and DNA degrades before reaching the  
462 seafloor, 3) microbes are more abundant in the near-bottom waters, either naturally or through mechanical  
463 disturbance resuspending sediment during the coring process, outnumbering groups that have been mixed  
464 in from overlaying water. Despite the presence of a plume and precipitation, a barrier between the sea  
465 floor and the water column biotopes is present, consistent with global broad scale non-vent benthic-  
466 pelagic patterns (Zinger et al., 2011). According to Khripounoff et al. (2001) particulate fall-out from the  
467 Rainbow plume is spatially very limited. This implies that the extended chemical imprint on the sediment  
468 (reported by Cave et al. (2002), Chavagnac et al. (2005), and this study), is likely to have formed when  
469 the plume is in direct contact with the sediment during its vertical tidal migration. As the plume rises  
470 again, the associated distinct communities apparently resume dominance in the near-bottom water.  
471 Though Epsilonproteobacteria have been detected in Rainbow vent sediments comprising over 5 % of the  
472 sediment community (Lopez-Garcia et al., 2003), very few reads of this group in sediment samples were  
473 present in our study probably as our coring samples were collected km's away from the venting site. Cave  
474 et al. (2002), observed chemical evolution of sediment composition with distance from source, thus we  
475 infer a relationship between the sediment dwelling Epsilonproteobacteria with nearby plume precipitates,

476 such as Cu and presumed precipitates Zn and Cd (Trocine and Trefry, 1988). Additionally, DNA  
477 degradation rate can be 7 to 100 times higher in sediment than in the water column (Dell'Anno and  
478 Corinaldesi, 2004). Therefore, although our results suggest no microbial plume community imprint on  
479 the sediment, we cannot rule out short lived episodic community changes when the plume is in contact  
480 with the sediment.

481

### 482 **4.3 Geochemical gradients within the hydrothermal plume**

483 Analysis of SPM in water samples taken along the flow path of the plume, as well as off the flow path,  
484 showed conspicuous trends of elements, reflecting the chemical evolution of the plume as it drifts away  
485 from its hydrothermal source.

486 The chalcophile elements (Cu, Co and Zn) were found to have the highest element/Fe molar ratios closest  
487 to the vent site, indicating either rapid removal from the hydrothermal plume or removal from the solid  
488 phase as the plume drifts away from the vent site. Using SEM-EDS, it was demonstrated that at the  
489 proximal downstream stations mainly Fe-sulfides were found, whereas Fe-(oxyhydr)oxides were found  
490 further downstream. This suggests that chalcophile elements are mainly present in the form of sulfide  
491 mineral particles at the proximal stations, which are entrained in the flow of hydrothermal water  
492 emanating from the Rainbow vents and subsequently rapidly lost by settling from the plume in sulfide-  
493 bearing phases, while a large portion of Fe remains in suspension (Cave et al., 2002; Edmonds and  
494 German, 2004), consistent with decreasing concentrations of Cu, Zn and Co in sediment recovered from  
495 the Rainbow area with increasing distance to the vent site (Cave et al., 2002).

496 The oxyanions (V and P) showed slightly varying element/Fe molar ratios with increasing distance away  
497 from Rainbow, suggesting co-precipitation with Fe as oxyhydroxides (Edmonds and German, 2004). No  
498 additional uptake of these elements was observed with increasing distance from the vent field (German  
499 et al., 1991), since these elements are scavenged initially in significant amounts during the buoyant plume  
500 phase (Cave et al., 2002).

501 The trend shown by Mn/Fe molar ratios can be attributed to the slower oxidation kinetics of Mn (Cave et  
502 al., 2002). It takes longer for reduced Mn to be oxidised than it would for Fe, resulting in an increase in  
503 particulate Mn with increasing distance from the Rainbow hydrothermal vent field, which subsequently  
504 settles out from the plume as Mn-oxyhydroxides (Cave et al., 2002).

505 The observed positive relationship between the REEs and Fe is indicative of continuous scavenging of  
506 these elements from the ambient seawater onto Fe-oxyhydroxides (Edmonds and German, 2004;  
507 Chavagnac et al., 2005; Caetano et al., 2013). Therefore, the highest element/Fe molar ratios were  
508 observed away from the Rainbow hydrothermal vent site, where Fe-(oxyhydr)oxides are dominant more  
509 distal to the vent site.

510 The Ca/Fe molar ratios vary between 0 and 15 for the stations downstream of the Rainbow hydrothermal  
511 vent, but are higher at the distant downstream station 47 and 49 and upstream stations 28 and 40.  
512 Especially at station 40, located on the Rainbow Ridge, the Ca/Fe molar ratio is significantly higher than  
513 at the other stations. This is in line with observations by Khripounoff et al. (2001) and Cave et al. (2002)  
514 who also found that the relative Ca concentration in settling particles and the sediments is lower close the  
515 Rainbow vent field and increases as the Fe concentration decreases when the plume disperses. Since Ca  
516 is naturally present in high abundances in pelagic skeletal carbonate which rains down from the overlying  
517 water column and Fe is mainly present as a hydrothermal component the Ca/Fe molar ratio could be an  
518 indicator for the extent of the hydrothermal influence. The high molar ratio at station 40 would then  
519 suggest that this station is hardly or not at all influenced by the hydrothermal plume as the natural  
520 abundance of particulate iron is low (e.g. Michard et al., 1984 and this study), whereas station 28, 47 and  
521 49 are, as expected, influenced in more moderate degrees compared with the stations directly downstream  
522 of Rainbow.

523

#### 524 **4.4 Microbial gradients within the hydrothermal plume**

525 The microbial plume community composition and diversity altered with distance from the plume source  
526 showcasing a horizontal heterogeneity within the plume. Despite dilution, the vent associated group

527 Epsilonproteobacteria (specifically the most common genus *Sulfurimonas*), appeared to dominate the  
528 community composition. This is likely due to its flexibility to exploit mainly sulfur compounds as electron  
529 donors, and oxygen and nitrate as acceptors (Nakagawa et al., 2005), making them suitable inhabitants of  
530 dynamic environments (Huber et al., 2003). From the relative abundance data presented here it cannot be  
531 determined whether Epsilonproteobacteria dominate by rapid reproduction or if other groups decline in  
532 abundance. However, it is evident that Epsilonproteobacteria remain competitive or outcompete other  
533 competitors such as generalists Gammaproteobacteria that are often vent associated (i.e. SUP05). It is  
534 unlikely that this pattern is caused by entrainment of Epsilonproteobacteria from background seawater  
535 over time. This is based on the lack of significant presence of Epsilonproteobacteria in above-plume water  
536 and at remote station 13, and reduced mixing that neutrally buoyant plumes generally experience  
537 (McCollom, 2000). This is further supported by the increasing uniqueness of the plume community with  
538 distance from the source, suggesting that mixing and entrainment between downstream biotopes is  
539 negligible.

540 The neutrally buoyant plume is likely too chemically enriched for non-adapted microbial taxa to thrive,  
541 and consequently are outcompeted by groups that can benefit from or tolerate the chemical nature of the  
542 plume. Therefore, it is likely that less specialised groups die out due to lack of appropriate resources and  
543 interspecies competition, as indicated by the decline in biodiversity with age of plume (distance) directly  
544 mirroring the increasing dominance of Epsilonproteobacteria, a group already known to influence  
545 diversity and community structures (Opatkiewicz et al., 2009; Sylvan et al., 2012). In addition, the  
546 decrease in concentration of particulate matter may influence microbial diversity (Huber et al., 2003).  
547 Temporal succession has been observed within plume environments by Sylvan et al., 2012 and Reed et  
548 al., 2015, driven by metabolic energy yield and concentration of the electron donors. These patterns may  
549 relate to ecological succession (Connell and Slaytor, 1977) within the plume with change in microbial  
550 communities resulting in a low diversity, climax plume community. At the distant stations 47 and 49, the  
551 community was less dominated by Epsilonproteobacteria and more diverse, indicating a gradual return to  
552 what is possibly a non-plume influenced state of the microbial community. The wide range of correlations  
553 within and between microbial classes and water properties, i.e. ranging from chemical to physical  
554 variables (Fig. S4), indicates a complex array of community drivers within the plume.

555 In contrast to our results, Sheik et al. (2015) and Djurhuus et al. (2017), observed decreasing  
556 Epsilonproteobacteria abundance within hundreds of metres from the source in the rising, buoyant portion  
557 of plumes generated by Indian Ocean and South Pacific vents. Interestingly, in our results  
558 Epsilonproteobacteria were least dominant in the neutrally buoyant plume closest to the Rainbow vent  
559 site, which may indicate that entrainment of other microbial groups within the rising portion of the plume  
560 initially dilutes the contribution of Epsilonproteobacteria, whilst the competitive advantage of this group  
561 becomes only evident at a later stage as the plume drifts away from the source. However, Huber et al.,  
562 2003 suggested that Epsilonproteobacteria, thrive in weaker diffuse flow due to lower temperature and  
563 great electron acceptor availability, suggesting greater habitat suitability away from the immediate  
564 venting orifice. Furthermore, it has been demonstrated that Epsilonproteobacteria (specifically  
565 *Sulfurimonas*) have higher dispersal capabilities than thermophilic vent associated microbial groups  
566 (Mino et al., 2017). A sampling design to follow the continuity of the plume from the buoyant to the  
567 neutrally buoyant portion would be a suitable approach to fully trace the evolution of the plume from the  
568 orifice to full dilution. However, the term full dilution is ambiguous as it is unknown exactly how far the  
569 plume influences the water properties and how far the plume associated bacteria will follow, adding water  
570 column microbial community heterogeneity beyond our study spatial extent.

571

#### 572 **4.5 Possible effects of SMS mining plumes**

573 Mining of SMS deposits will create additional plumes generated by activities of mining vehicles  
574 (resuspension) and by the discharge of solids from the surface vessel (discharge plume). It is yet unknown  
575 how these plumes will affect the ecosystem at active and inactive hydrothermal vent sites. Our study  
576 showed the influence of a natural hydrothermal plume on the pelagic microbial and chemical composition  
577 up to 25 km away from its source. Not unlikely, the dispersion of sediment and chemically reactive  
578 mineral material in the water column may cause similar or larger changes to the background state.

579 While large particles mobilised by mining are expected to stay close to the seafloor and settle out rapidly,  
580 smothering fauna in the immediate surroundings (Jones et al., 2018), smaller particles will disperse  
581 further, potentially invoking effects on a larger spatial scale. Modelling the behaviour of the discharge

582 plume generated by the proposed Solwara 1 SMS mining has shown that these plumes can extend up to  
583 10 km from the mining site, resulting in a deposit thickness of up to 50 cm within 1 km of the discharge  
584 site (Gwyther et al., 2008; Boschen et al., 2013). Apart from the physical impact that suspended fine-  
585 grained solids may have especially on suspension feeders, the presence of chemically reactive material  
586 may give the mining plume a distinct chemical and microbial fingerprint, analogues to a certain context  
587 to what we observed in the natural plume.

588 The extent of the local impact of deep-sea mining will depend on the location where the mining takes  
589 place. At an active site like the Rainbow hydrothermal vent field, we showed that even in the distant  
590 plume (25 km away from Rainbow) hydrothermal plume microbiota dominate. When a mining discharge  
591 plume at an active hydrothermal vent field would be merged with the natural plume, the local effects  
592 might be minimal since microbial communities are already adapted to the metal-rich environments  
593 (Gwyther et al., 2008). However, a mining plume consisting of a dense suspension of bottom sediment  
594 and fine-grained metal sulfides is expected to support an altered microbial community in terms of  
595 abundance and composition, impacting the hydrothermal plume community. Moreover, the effects over  
596 larger spatial scales could be multiplied because of the increased export of electron donors by mining  
597 activities. Reed et al. (2015), who studied a hydrothermal plume in the Lau basin, have shown that the  
598 export of the chemolithoautotrophs from a plume increases with increasing availability of electron donors.  
599 Dispersion of chemolithoautotrophs is variable between groups depending on the energetics of their  
600 metabolisms, for example, methanotrophs which could disperse more than 50 km, are likely to disperse  
601 further than sulfur oxidisers (Reed et al., 2015). Increased export of microbial biomass from plumes may  
602 have impact on other marine systems which are hospitable to chemolithoautotrophs, such as oxygen  
603 minimum zones (Dick et al., 2013) and to higher trophic levels (Phillips, 2017). At inactive sites the effect  
604 on the background fauna is also potentially large since these are not adapted to the heavy metal rich  
605 environments and the discharge plume could prove to be toxic to the fauna (Boschen et al., 2013), possibly  
606 affecting organisms at all levels of the food chain (Weaver et al., 2018). In addition, in case of multiple  
607 plumes at different depths due to stratification and vertical migration due to tidal regimes, the impacts  
608 may not be confined to a single depth band and may affect a large part of the water column, including  
609 other habitats, such as benthic habitats.

610

## 611 **5 Conclusion**

612 Our results demonstrate geochemically enriched plumes provide a dynamic habitat that is conducive to  
613 ecological changes in a short time span. Combining microbial and chemical analysis has proven to be a  
614 sensitive tool which enabled us to trace the hydrothermal plume up to 25 km downstream from the vent  
615 source and also upstream of the Rainbow vent site, implying that the influence of the hydrothermal vent  
616 on the surrounding environment may reach further than previously thought. The neutrally buoyant plume  
617 was chemically enriched which spawned a distinct microbial biotope dominated by vent associated  
618 species. As the plume aged and dispersed we observed alteration of the chemical composition and  
619 microbial community composition of the plume, showcasing a horizontal heterogeneous plume. Overall  
620 we have shown that a hydrothermal plume acts as a unique chemically enriched environment where  
621 distinct and variable microbial habitats are present. The plume heterogeneity and its dynamical behaviour  
622 would require extensive sampling in order to be able to assess the impacts and interferences by man-made  
623 mining plumes on the natural conditions.

624

## 625 **Data availability**

626 CTD data presented in this work, filter weights for SPM sampling, geochemical data of the (trace) metals  
627 and REE, associated calculated enrichment factors and information on the blanks, drift measurements and  
628 detection limits of the HR-ICP MS analyses will be submitted to PANGAEA when the paper is published  
629 and are also available in the NIOZ data portal (<https://dataverse.nioz.nl/dataverse/doi> under DOI  
630 10.25850/nioz/7b.b.s). Raw sequence data will be available via the European Nucleotide Archive (ENA)  
631 under accession number PRJEBXXXXX, once the paper is published.

632

633

634

635 **Author contribution**

636 GD, HDS, and FM conceptualised the study and undertook data collection. SH and DP undertook sample  
637 processing and analysis with contributions from and under the supervision of FM, GD, GJR, HDS, JvB  
638 and HW. SH and DP wrote the manuscript with contributions from all co-authors.

639

640 **Competing interests**

641 The authors declare that they have no conflict of interest.

642

643 **Acknowledgements**

644 This study was carried out in the framework of the TREASURE (Towards Responsible ExtrAction of  
645 SUBmarine RESources) project, funded (grant number 13273) by the Applied and Engineering Sciences  
646 (AES) domain of the Netherlands Organisation for Scientific Research (NWO) and by partners from the  
647 Dutch maritime industry. Topsector Water, a collaborative effort of Dutch industry, academia and  
648 government, funded ship time. We thank Evaline van Weerlee for assistance in DNA extraction and  
649 Patrick Laan for assistance in the chemical analysis of the collected samples. We also thank the crew and  
650 captain of the RV *Pelagia*, as well as NIOZ technicians for their essential assistance during cruise  
651 64PE398. SH received funding from the Blue Nodules project, EC grant agreement. 688785. DP is  
652 supported by the Natural Environmental Research Council [grant number NE/N012070/1]. HdS received  
653 funding from TREASURE. FM is supported financially by the Innovational Research Incentives Scheme  
654 of the Netherlands Organisation for Scientific Research (NWO-VIDI grant 016.161.360).

655

656 **References**

657 Agogue, H., Lamy, D., Neal, P. R., Sogin, M. L., and Herndl, G. J.: Water mass-specificity of bacterial communities  
658 in the North Atlantic revealed by massively parallel sequencing, *Mol Ecol*, 20, 258-274,  
659 <https://doi.org/10.1111/j.1365-294X.2010.04932.x> , 2011.

660 Anantharaman, K., Breier, J. A., and Dick, G. J.: Metagenomic resolution of microbial functions in deep-sea  
661 hydrothermal plumes across the Eastern Lau Spreading Center, *Isme J*, 10, 225-239,  
662 <https://doi.org/10.1038/ismej.2015.81>, 2016.

663 Boschen, R. E., Rowden, A. A., Clark, M. R., and Gardner, J. P. A.: Mining of deep-sea seafloor massive sulfides:  
664 A review of the deposits, their benthic communities, impacts from mining, regulatory frameworks and management  
665 strategies, *Ocean Coast Manage*, 84, 54-67, <https://doi.org/10.1016/j.ocecoaman.2013.07.005>, 2013.

666 Breier, J. A., Toner, B. M., Fakra, S. C., Marcus, M. A., White, S. N., Thurnherr, A. M., & German, C. R.: Sulfur,  
667 sulfides, oxides and organic matter aggregated in submarine hydrothermal plumes at 9 50' N East Pacific Rise.  
668 *Geochim. Cosmochim. Acta*, 88, 216-236, <https://doi.org/10.1016/j.gca.2012.04.003>, 2012.

669 Caetano, M., Vale, C., Anes, B., Raimundo, J., Drago, T., Schimdt, S., Nogueira, M., Oliveira, A., and Prego, R.:  
670 The Condor seamount at Mid-Atlantic Ridge as a supplementary source of trace and rare earth elements to the  
671 sediments, *Deep-Sea Res Pt II*, 98, 24-37, <https://doi.org/10.1016/j.dsr2.2013.01.009>, 2013.

672 Cave, R. R., German, C. R., Thomson, J., and Nesbitt, R. W.: Fluxes to sediments underlying the Rainbow  
673 hydrothermal plume at 36 degrees 14' N on the Mid-Atlantic Ridge, *Geochim Cosmochim Ac*, 66, 1905-1923,  
674 [https://doi.org/10.1016/S0016-7037\(02\)00823-2](https://doi.org/10.1016/S0016-7037(02)00823-2), 2002.

675 Cerqueira, T., Barroso, C., Froufe, H., Egas, C., and Bettencourt, R.: Metagenomic Signatures of Microbial  
676 Communities in Deep-Sea Hydrothermal Sediments of Azores Vent Fields, *Microb Ecol*, 76, 387-403,  
677 <https://doi.org/10.1007/s00248-018-1144-x>, 2018.

678 Charlou, J. L., Donval, J. P., Fouquet, Y., Jean-Baptiste, P., and Holm, N.: Geochemistry of high H<sub>2</sub> and CH<sub>4</sub> vent  
679 fluids issuing from ultramafic rocks at the Rainbow hydrothermal field (36 degrees 14' N, MAR), *Chem Geol*, 191,  
680 345-359, [https://doi.org/10.1016/S0009-2541\(02\)00134-1](https://doi.org/10.1016/S0009-2541(02)00134-1), 2002.

681 Chavagnac, V., German, C. R., Milton, J. A., and Palmer, M. R.: Sources of REE in sediment cores from the  
682 Rainbow vent site (36 degrees 14' N, MAR), *Chem Geol*, 216, 329-352, [https://doi.org/10.1016/S0009-2541\(02\)00134-1](https://doi.org/10.1016/S0009-2541(02)00134-1), 2005.

684 Clarke, K. R., Gorley, R. N.: PRIMER v6: User Manual/Tutorial (Plymouth Routines in Multivariate Ecological  
685 Research), PRIMER-E, Plymouth, 2006

686 Collins, P. C., Croot, P., Carlsson, J., Colaço, A., Grehan, A., Hyeong, K., Kennedy, R., Mohn, C., Smith, S., and  
687 Yamamoto, H.: A primer for the Environmental Impact Assessment of mining at seafloor massive sulfide deposits,  
688 *Mar Policy*, 42, 198-209, <https://doi.org/10.1016/j.marpol.2013.01.020>, 2013.

689 Connell, J. H., and Slayter, R. O.: Mechanisms of Succession in Natural Communities and Their Role in  
690 Community Stability and Organization, *Am Nat*, 111, 1119-1144, <https://doi.org/10.1086/283241>, 1977.

691 Cowen, J. P., and Bruland, K. W.: Metal Deposits Associated with Bacteria - Implications for Fe and Mn Marine  
692 Biogeochemistry, *Deep-Sea Res*, 32, 253-&, [https://doi.org/10.1016/0198-0149\(85\)90078-0](https://doi.org/10.1016/0198-0149(85)90078-0), 1985.

693 Cowen, J. P., Massoth, G. J., and Feely, R. A.: Scavenging Rates of Dissolved Manganese in a Hydrothermal Vent  
694 Plume, *Deep-Sea Res*, 37, 1619-1637, [https://doi.org/10.1016/0198-0149\(90\)90065-4](https://doi.org/10.1016/0198-0149(90)90065-4), 1990.

695 Dell'Anno, A., and Corinaldesi, C.: Degradation and turnover of extracellular DNA in marine sediments: Ecological  
696 and methodological considerations, *Appl Environ Microb*, 70, 4384-4386,  
697 <https://doi.org/10.1128/AEM.70.7.4384-4386.2004>, 2004.

698 Dick, G. J., Clement, B. G., Webb, S. M., Fodrie, F. J., Bargar, J. R., and Tebo, B. M.: Enzymatic microbial Mn(II)  
699 oxidation and Mn biooxide production in the Guaymas Basin deep-sea hydrothermal plume, *Geochim Cosmochim*  
700 *Ac*, 73, 6517-6530, <https://doi.org/10.1016/j.gca.2009.07.039>, 2009.

701 Dick, G. J., and Tebo, B. M.: Microbial diversity and biogeochemistry of the Guaymas Basin deep-sea  
702 hydrothermal plume, *Environ Microbiol*, 12, 1334-1347, <https://doi.org/10.1111/j.1462-2920.2010.02177.x>, 2010.

703 Dick, G. J., Anantharaman, K., Baker, B. J., Li, M., Reed, D. C., and Sheik, C. S.: The microbiology of deep-sea  
704 hydrothermal vent plumes: ecological and biogeographic linkages to seafloor and water column habitats, *Front*  
705 *Microbiol*, 4, <https://doi.org/10.3389/fmicb.2013.00124>, 2013.

706 Djurhuus, A., Mikalsen, S. O., Giebel, H. A., and Rogers, A. D.: Cutting through the smoke: the diversity of  
707 microorganisms in deep-sea hydrothermal plumes, *Royal Society Open Science*, 4,  
708 <https://doi.org/10.1098/rsos.160829>, 2017.

709 Douville, E., Charlou, J. L., Oelkers, E. H., Bienvenu, P., Colon, C. F. J., Donval, J. P., Fouquet, Y., Prieur, D.,  
710 and Appriou, P.: The rainbow vent fluids (36 degrees 14' N, MAR): the influence of ultramafic rocks and phase  
711 separation on trace metal content in Mid-Atlantic Ridge hydrothermal fluids, *Chem Geol*, 184, 37-48,  
712 [https://doi.org/10.1016/S0009-2541\(01\)00351-5](https://doi.org/10.1016/S0009-2541(01)00351-5), 2002.

713 Edmonds, H. N., and German, C. R.: Particle geochemistry in the Rainbow hydrothermal plume, Mid-Atlantic  
714 Ridge, *Geochim Cosmochim Acta*, 68, 759-772, [https://doi.org/10.1016/S0016-7037\(03\)00498-8](https://doi.org/10.1016/S0016-7037(03)00498-8), 2004.

715 Emery, W. J., and Meincke, J.: Global Water Masses - Summary and Review, *Oceanol Acta*, 9, 383-391, 0399-  
716 1784/86/04, 1986.

717 Findlay, A. J., Gartman, A., Shaw, T. J., and Luther, G. W.: Trace metal concentration and partitioning in the first  
718 1.5 m of hydrothermal vent plumes along the Mid-Atlantic Ridge: TAG, Snakepit, and Rainbow, *Chem Geol*, 412,  
719 117-131, <https://doi.org/10.1016/j.chemgeo.2015.07.021>, 2015.

720 Fouquet, Y., Barriga, F., Charlou, J. L., Elderfield, H., German, C. R., Ondréas, H., Parson, L., Radford-Knoery,  
721 J., Relvas, J., Ribeiro, A., Schultz, A., Apprioual, R., Cambon, P., Costa, I., Donval, J. P., Douville, E., Landuré,  
722 J. Y., Normund, A., Pellé, H., Ponsevera, E., Riches, S., Santana, H., and Stephan, M.: Flores diving cruise with  
723 the Nautilé near the Azores. First dives on the Rainbow field: hydrothermal seawater/mantle interaction, *InterRidge*  
724 *News*, 7, 24-28, 1998.

725 Frank, K. L., Rogers, D. R., Olins, H. C., Vidoudez, C., and Girguis, P. R.: Characterizing the distribution and rates  
726 of microbial sulfate reduction at Middle Valley hydrothermal vents, *Isme J*, 7, 1391-1401,  
727 <https://doi.org/10.1038/ismej.2013.17>, 2013.

728 German, C. R., Campbell, A. C., and Edmond, J. M.: Hydrothermal Scavenging at the Mid-Atlantic Ridge -  
729 Modification of Trace-Element Dissolved Fluxes, *Earth and Planetary Science Letters*, 107, 101-114,  
730 [https://doi.org/10.1016/0012-821X\(91\)90047-L](https://doi.org/10.1016/0012-821X(91)90047-L), 1991.

731 German, C. R., Klinkhammer, G. P., and Rudnicki, M. D.: The Rainbow hydrothermal plume, 36 degrees 15'N,  
732 MAR, *Geophys Res Lett*, 23, 2979-2982, <https://doi.org/10.1029/96GL02883>, 1996.

733 German, C. R., Richards, K. J., Rudnicki, M. D., Lam, M. M., Charlou, J. L., and Party, F. S.: Topographic control  
734 of a dispersing hydrothermal plume, *Earth and Planetary Science Letters*, 156, 267-273,  
735 [https://doi.org/10.1016/S0012-821X\(98\)00020-X](https://doi.org/10.1016/S0012-821X(98)00020-X), 1998.

736 Gwyther, D., and Wright, M.: Environmental Impact Statement: Solwara 1, Coffey Natural Systems Pty Ltd, 47-  
737 65, 2008.

738 Han, Y. C., Gonnella, G., Adam, N., Schippers, A., Burkhardt, L., Kurtz, S., Schwarz-Schampera, U., Franke, H.,  
739 and Perner, M.: Hydrothermal chimneys host habitat-specific microbial communities: analogues for studying the

740 possible impact of mining seafloor massive sulfide deposits, *Sci Rep-Uk*, 8, [https://doi.org/10.1038/s41598-018-](https://doi.org/10.1038/s41598-018-28613-5)  
741 28613-5, 2018.

742 Huber, J. A., Butterfield, D. A. and Baross, J. A.: Bacterial diversity in a subseafloor habitat following a deep-sea  
743 volcanic eruption. *FEMS Microbiol Ecol*, 43(3), pp.393-409, <https://doi.org/10.1111/j.1574-6941.2003.tb01080.x>,  
744 2003.

745 Hoagland, P., Beaulieu, S., Tivey, M. A., Eggert, R. G., German, C., Glowka, L., and Lin, J.: Deep-sea mining of  
746 seafloor massive sulfides, *Mar Policy*, 34, 728-732, <https://doi.org/10.1016/j.marpol.2009.12.001>, 2010.

747 Jannasch, H. W., and Mottl, M. J.: Geomicrobiology of Deep-Sea Hydrothermal Vents, *Science*, 229, 717-725,  
748 <https://doi.org/10.1126/science.229.4715.717>, 1985.

749 Jones, D. O. B., Amon, D. L., and Chapman, A. S. A.: Mining Deep-Ocean Mineral Deposits: What are the  
750 Ecological Risks?, *Elements*, 14, 325-330, <https://doi.org/10.2138/gselements.14.5.325>, 2018.

751 Khripounoff, A., Vangriesheim, A., Crassous, P., Segonzac, M., Colaco, A., Desbruyeres, D., and Barthelemy, R.:  
752 Particle flux in the Rainbow hydrothermal vent field (Mid-Atlantic Ridge): Dynamics, mineral and biological  
753 composition, *J Mar Res*, 59, 633-656, <https://doi.org/10.1357/002224001762842217>, 2001.

754 Levin, L. A., Mengerink, K., Gjerde, K. M., Rowden, A. A., Van Dover, C. L., Clark, M. R., Ramirez-Llodra, E.,  
755 Currie, B., Smith, C. R., Sato, K. N., Gallo, N., Sweetman, A. K., Lily, H., Armstrong, C. W., and Brider, J.:  
756 Defining “Serious Harm” to the Marine Environment in the Context of Deep-Seabed Mining, *Marine Policy*, 245-  
757 59, <http://dx.doi.org/10.1016/j.marpol.2016.09.032>, 2016

758 Lopez-Garcia, P., Philippe, H., Gail, F., and Moreira, D.: Autochthonous eukaryotic diversity in hydrothermal  
759 sediment and experimental microcolonizers at the Mid-Atlantic Ridge, *P Natl Acad Sci USA*, 100, 697-702,  
760 <https://doi.org/10.1073/pnas.0235779100>, 2003.

761 Ludford, E. M., Palmer, M. R., German, C. R., and Klinkhammer, G. P.: The geochemistry of Atlantic hydrothermal  
762 particles, *Geophys Res Lett*, 23, 3503-3506, <https://doi.org/10.1029/96GL02078>, 1996.

763 Mandernack, K. W., and Tebo, B. M.: Manganese Scavenging and Oxidation at Hydrothermal Vents and in Vent  
764 Plumes, *Geochim Cosmochim Ac*, 57, 3907-3923, [https://doi.org/10.1016/0016-7037\(93\)90343-U](https://doi.org/10.1016/0016-7037(93)90343-U), 1993.

765 Marques, A. F. A., Barriga, F., Chavagnac, V. and Fouquet, Y. : Mineralogy, geochemistry, and Nd isotope  
766 composition of the Rainbow hydrothermal field, Mid-Atlantic Ridge, Mineralium Deposita, 41, 52-67,  
767 <https://doi.org/10.007/s00126-005-0040-8>, 2006.

768 McCollom, T. M.: Geochemical constraints on primary productivity in submarine hydrothermal vent plumes, Deep-  
769 Sea Res Pt I, 47, 85-101, [https://doi.org/10.1016/S0967-0637\(99\)00048-5](https://doi.org/10.1016/S0967-0637(99)00048-5), 2000.

770 Michard, G., Albarède, F., Michard, A., Minister, J. F., Charlou, J. L., and Tan, N.: Chemistry of Solution from the  
771 13 degrees N East Pacific Rise Hydrothermal Site. Earth and Planetary Science Letters 67, 297-307,  
772 [https://doi.org/10.1016/0012-821X\(84\)90169-9](https://doi.org/10.1016/0012-821X(84)90169-9), 1984

773 Mino, S., Nakagawa, S., Makita, H., Toki, T., Miyazaki, J., Sievert, S. M., ... & Watanabe, H.: Endemicity of the  
774 cosmopolitan mesophilic chemolithoautotroph *Sulfurimonas* at deep-sea hydrothermal vents. The ISME journal,  
775 11(4), 909, <https://doi.org/10.1038/ismej.2016.178>, 2017.

776 Nakagawa, S., Takai, K., Inagaki, F., Hirayama, H., Nunoura, T., Horikoshi, K., and Sako, Y.: Distribution,  
777 phylogenetic diversity and physiological characteristics of epsilon-Proteobacteria in a deep-sea hydrothermal field,  
778 *Environ Microbiol*, 7, 1619-1632, <https://doi.org/10.1111/j.1462-2920.2005.00856.x>, 2005.

779 Olins, H. C., Rogers, D. R., Preston, C., Ussler, W., Pargett, D., Jensen, S., Roman, B., Birch, J. M., Scholin, C.  
780 A., Haroon, M. F., and Girguis, P. R.: Co-registered Geochemistry and Metatranscriptomics Reveal Unexpected  
781 Distributions of Microbial Activity within a Hydrothermal Vent Field, *Front Microbiol*, 8,  
782 <https://doi.org/10.3389/fmicb.2017.01042>, 2017.

783 Opatkiewicz, A. D., Butterfield, D. A., and Baross, J. A.: Individual hydrothermal vents at Axial Seamount harbor  
784 distinct seafloor microbial communities, *Fems Microbiol Ecol*, 70, 413-424, <https://doi.org/10.1111/j.1574-6941.2009.00747.x>, 2009.

786 Orcutt, B. N., Sylvan, J. B., Knab, N. J., & Edwards, K. J.: Microbial ecology of the dark ocean above, at, and  
787 below the seafloor. *Microbiol. Mol. Biol. Rev.*, 75(2), 361-422, <https://doi.org/10.1128/MMBR.00039-10>, 2011.

788 Phillips, B. T.: Beyond the vent: New perspectives on hydrothermal plumes and pelagic biology, *Deep-Sea Res Pt*  
789 *Ii*, 137, 480-485, <https://doi.org/10.1016/j.dsr2.2016.10.005>, 2017.

790 Ramirez-Llodra, E., Tyler, P. A., Baker, M. C., Bergstad, O. A., Clark, M. R., Escobar, E., Levin, L. A., Menot,  
791 L., Rowden, A. A., Smith, C. R., and Van Dover, C. L.: Man and the Last Great Wilderness: Human Impact on the  
792 Deep Sea, *Plos One*, 6, <https://doi.org/10.1371/journal.pone.0022588>, 2011.

793 Reed, D. C., Breier, J. A., Jiang, H. S., Anantharaman, K., Klausmeier, C. A., Toner, B. M., Hancock, C., Speer,  
794 K., Thurnherr, A. M., and Dick, G. J.: Predicting the response of the deep-ocean microbiome to geochemical  
795 perturbations by hydrothermal vents, *Isme J*, 9, 1857-1869, <https://doi.org/10.1038/ismej.2015.4>, 2015.

796 Resing, J. A., P. N. Sedwick, C. R. German, W. J. Jenkins, J. W. Moffett, B. M. Sohst, and A. Tagliabue.: Basin-  
797 Scale Transport of Hydrothermal Dissolved Metals across the South Pacific Ocean. *Nature* 523, no. 7559, 200-3.  
798 <http://dx.doi.org/10.1038/nature14577>, 2015.

799 Severmann, S., Johnson, C. M., Beard, B. L., German, C. R., Edmonds, H. N., Chiba, H., and Green, D. R. H.: The  
800 effect of plume processes on the Fe isotope composition of hydrothermally derived Fe in the deep ocean as inferred  
801 from the Rainbow vent site, Mid-Atlantic Ridge, 36 degrees 14' N, *Earth and Planetary Science Letters*, 225, 63-  
802 76, <https://doi.org/10.1016/j.epsl.2004.06.001>, 2004.

803 Sheik, C. S., Anantharaman, K., Breier, J. A., Sylvan, J. B., Edwards, K. J., and Dick, G. J.: Spatially resolved  
804 sampling reveals dynamic microbial communities in rising hydrothermal plumes across a back-arc basin, *Isme J*,  
805 9, 1434-1445, <https://doi.org/10.1038/ismej.2014.228>, 2015.

806 Sunamura, M., Higashi, Y., Miyako, C., Ishibashi, J., and Maruyama, A.: Two bactetia phylotypes are predominant  
807 in the Suiyo Seamount hydrothermal plume, *Appl Environ Microb*, 70, 1190-1198,  
808 <https://doi.org/10.1128/AEM.70.2.1190-1198.2004>, 2004.

809 Sylvan, J. B., Pyenson, B. C., Rouxel, O., German, C. R., & Edwards, K. J.: Time-series analysis of two  
810 hydrothermal plumes at 9° 50' N East Pacific Rise reveals distinct, heterogeneous bacterial populations.  
811 *Geobiology*, 10(2), 178-192, <https://doi.org/10.1111/j.1472-4669.2011.00315.x>, 2012.

812 Thurnherr, A. M., and Richards, K. J.: Hydrography and high-temperature heat flux of the Rainbow hydrothermal  
813 site (36 degrees 14 ' N, Mid-Atlantic Ridge), *J Geophys Res-Oceans*, 106, 9411-9426,  
814 <https://doi.org/10.1029/2000JC900164>, 2001.

815 Thurnherr, A. M., Richards, K. J., German, C. R., Lane-Serff, G. F., and Speer, K. G.: Flow and mixing in the rift  
816 valley of the Mid-Atlantic Ridge, *J Phys Oceanogr*, 32, 1763-1778, [https://doi.org/10.1175/1520-0485\(2002\)032<1763:FAMITR>2.0.CO;2](https://doi.org/10.1175/1520-0485(2002)032<1763:FAMITR>2.0.CO;2), 2002.

818 Trocine, R. P. and Trefry, J. H.: Distribution and chemistry of suspended particles from an active hydrothermal  
819 vent site on the Mid-Atlantic Ridge at 26 °N, *Earth and Planetary Science Letters* 88, 1-15,  
820 [https://doi.org/10.1016/0012-821X\(88\)90041-6](https://doi.org/10.1016/0012-821X(88)90041-6), 1988.

821 van Bleijswijk, J. D. L., Whalen, C., Duineveld, G. C. A., Lavaleye, M. S. S., Witte, H. J., and Mienis, F.: Microbial  
822 assemblages on a cold-water coral mound at the SE Rockall Bank (NE Atlantic): interactions with hydrography  
823 and topography, *Biogeosciences*, 12, 4483-4496, <https://doi.org/10.5194/bg-12-4483-2015>, 2015.

824 van Haren, H., Duineveld, G., and de Stigter, H.: Prefrontal bore mixing, *Geophys Res Lett*, 44, 9408-9415,  
825 <https://doi.org/10.1002/2017GL074384>, 2017.

826 Vare, L. L., Baker, M. C., Howe, J. A., Levin, L. A., Neira, C., Ramirez-Llodra, E. Z., Reichelt-Brushett, A.,  
827 Rowden, A. A., Shimmield, T. M., Simpson, S. L., and Soto, E. H.: Scientific Considerations for the Assessment  
828 and Management of Mine Tailings Disposal in the Deep Sea, *Frontiers in Marine Science*, 5,  
829 <https://doi.org/10.3389/fmars.2018.00017>, 2018.

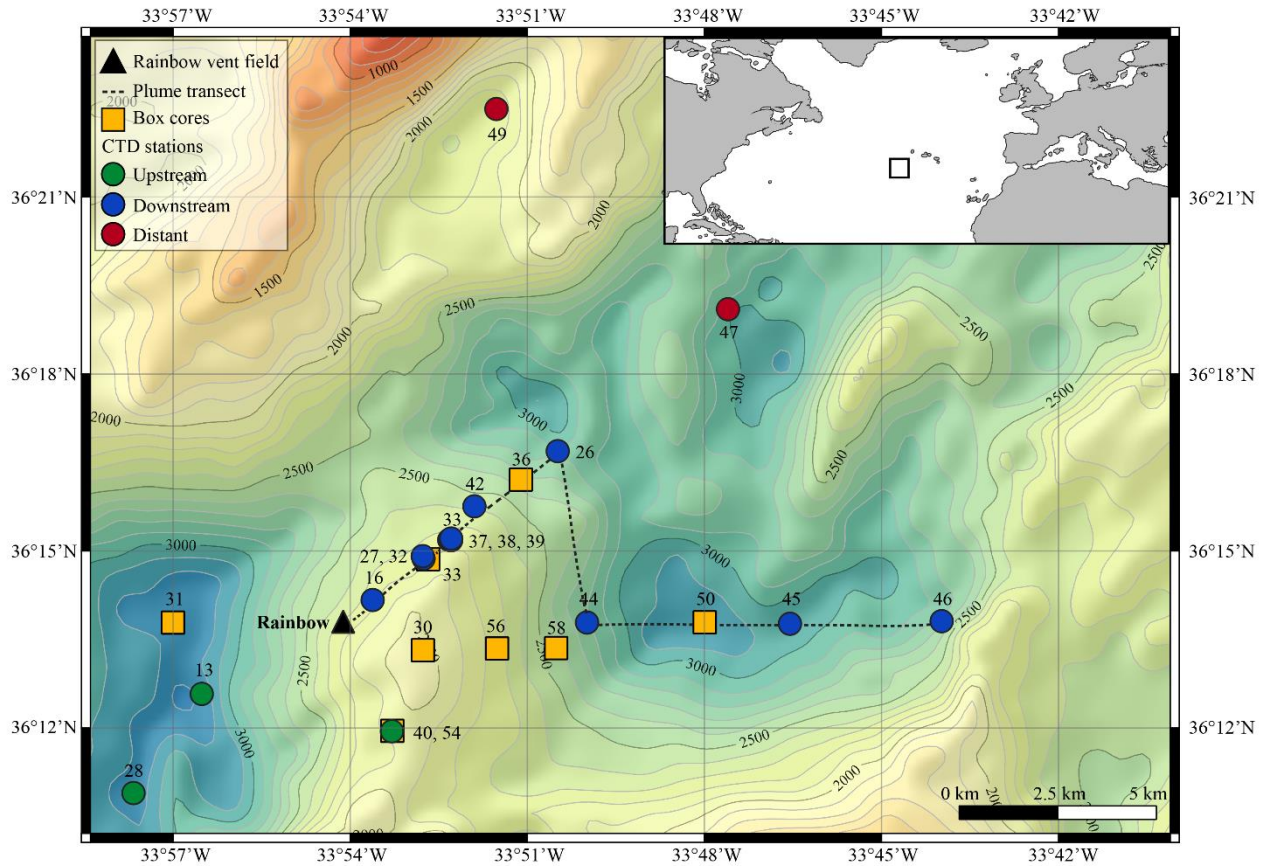
830 Weaver, P. P., Billett, D. S., and Van Dover, C. L.: Environmental risks of deep-sea mining, in: *Handbook on*  
831 *Marine Environment Protection*, Springer, 215-245, [https://doi.org/10.1007/978-3-319-60156-4\\_11](https://doi.org/10.1007/978-3-319-60156-4_11), 2018.

832 Wetzel, L. R., and Shock, E. L.: Distinguishing ultramafic- from basalt-hosted submarine hydrothermal systems  
833 by comparing calculated vent fluid compositions, *J Geophys Res-Sol Ea*, 105, 8319-8340,  
834 <https://doi.org/10.1029/1999JB900382>, 2000.

835 Yilmaz, P., Parfrey, L.W., Yarza, P., Gerken, J., Pruesse, E., Quast, C., Schweer, T., Peplies, J., Ludwig, W. and  
836 Glöckner, F.O.: The SILVA and “all-species living tree project (LTP)” taxonomic frameworks. *Nucleic Acids Res*,  
837 42(D1), pp.D643-D648, <https://doi.org/10.1093/nar/gkt1209>, 2014.

838 Zinger, L., Amaral-Zettler, L. A., Fuhrman, J. A., Horner-Devine, M. C., Huse, S. M., Welch, D. B. M., Martiny,  
839 J. B. H., Sogin, M., Boetius, A., and Ramette, A.: Global Patterns of Bacterial Beta-Diversity in Seafloor and  
840 Seawater Ecosystems, *Plos One*, 6, <https://doi.org/10.1371/journal.pone.0024570>, 2011.

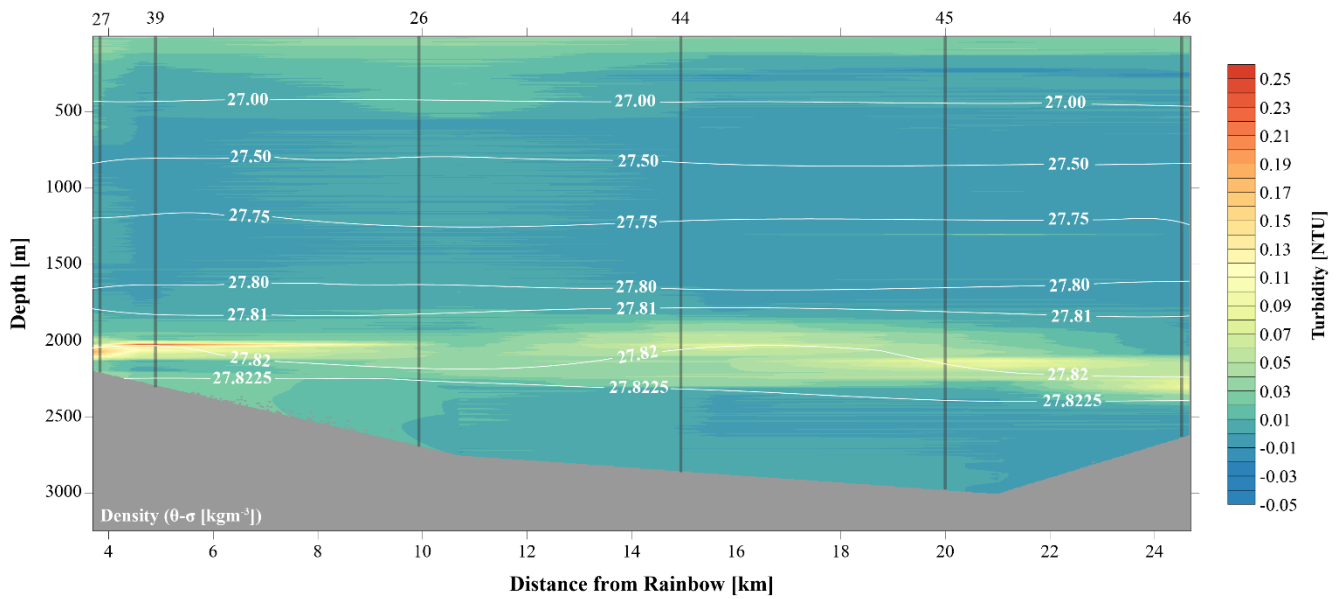
841



843

844 *Figure 1: Geographical location (inset) and bathymetric map of the Rainbow study site on the Mid Atlantic Ridge*  
 845 *(from EMOD data base) with sampling locations depicted.*

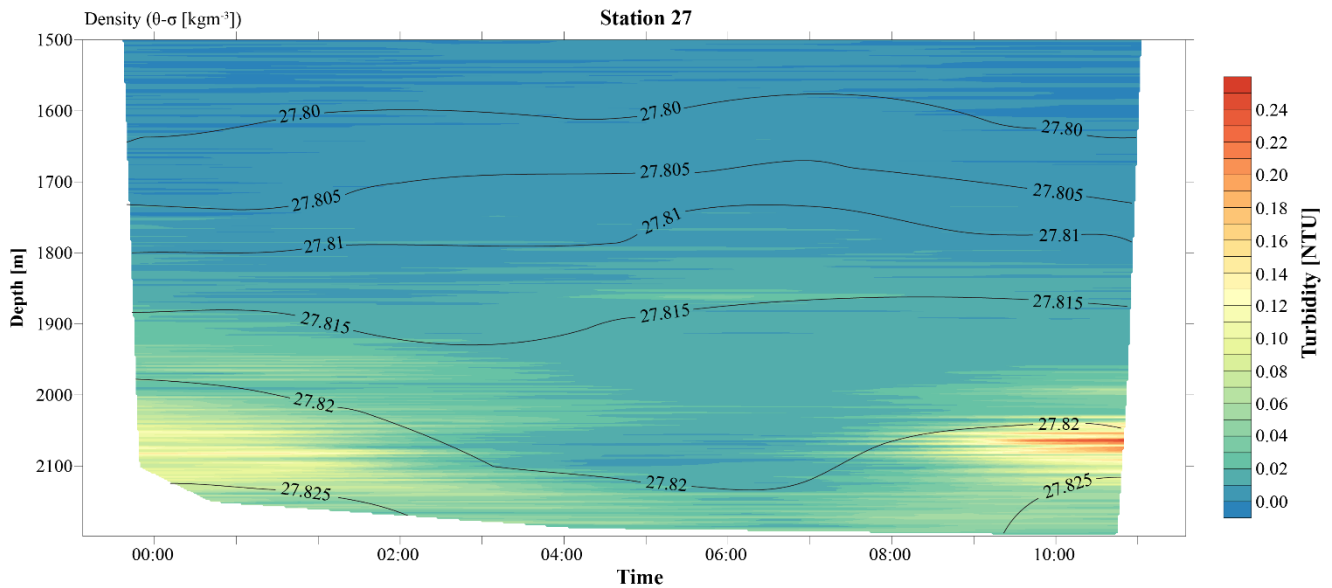
846



847

848 *Figure 2: Transect along main plume path (indicated in Fig. 1 as plume transect), showing turbidity in the water*  
 849 *column. The plume is indicated by highest turbidity values and disperses away from the Rainbow vent field.*

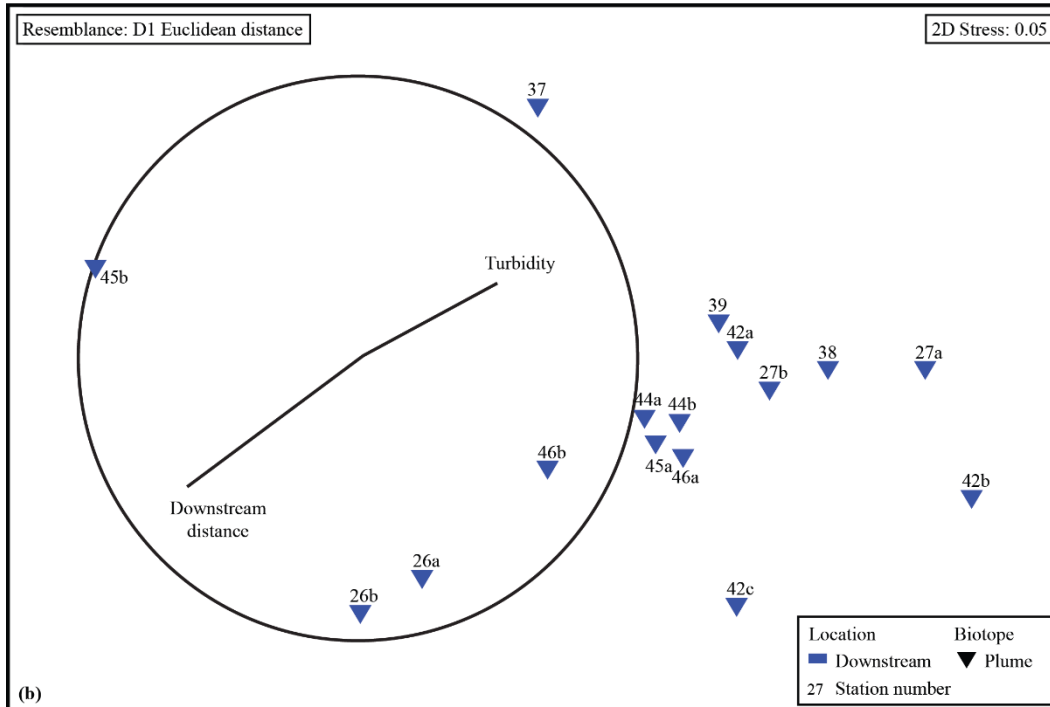
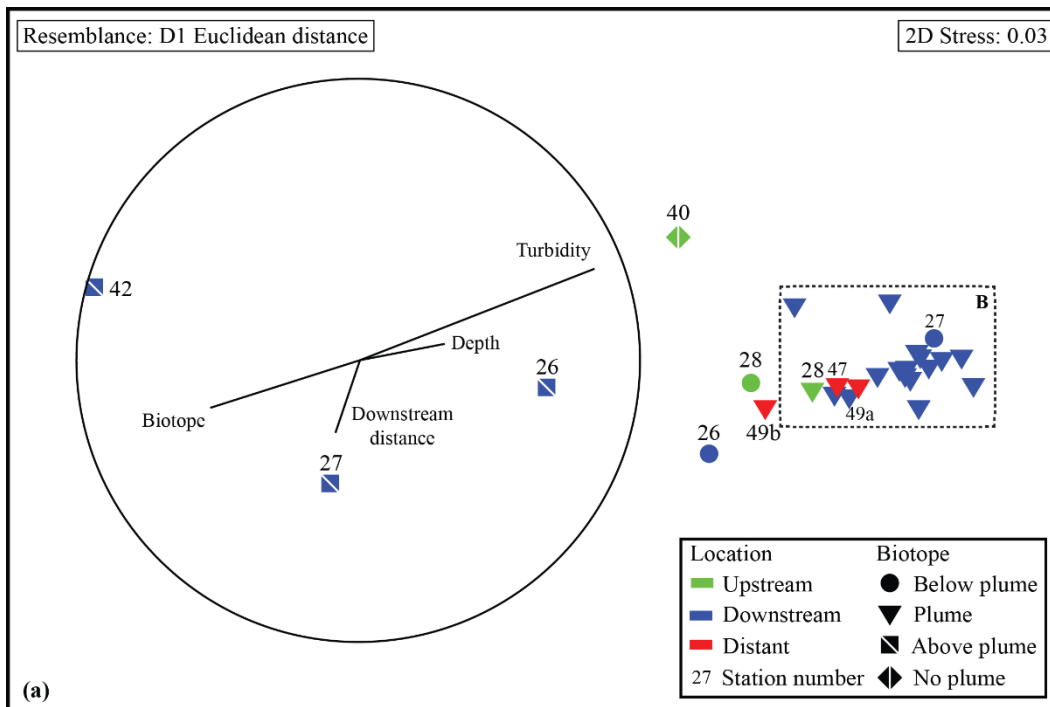
850



851

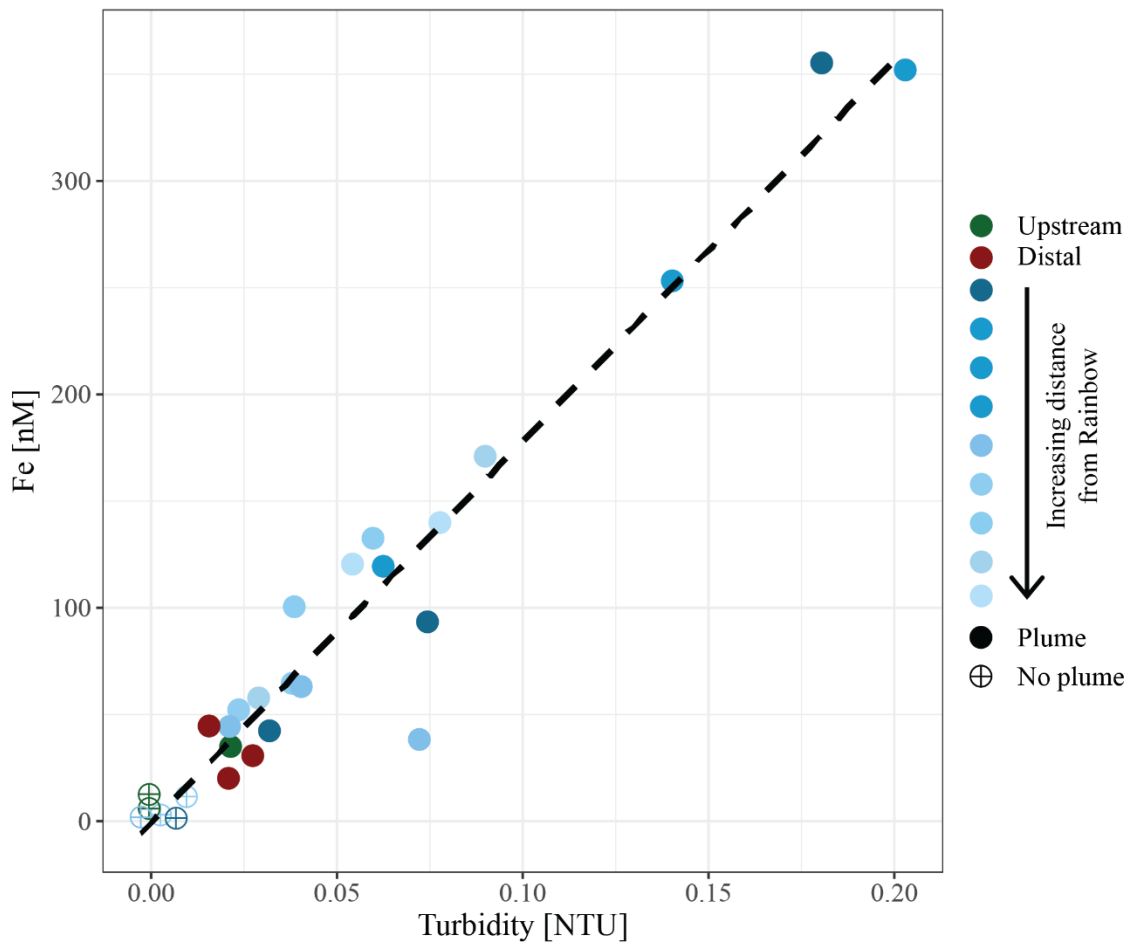
852 *Figure 3: 12 hour CTD YOYO casts at station 27 showing the temporal evolution of the hydrothermal plume over*  
 853 *a tidal cycle.*

854



855

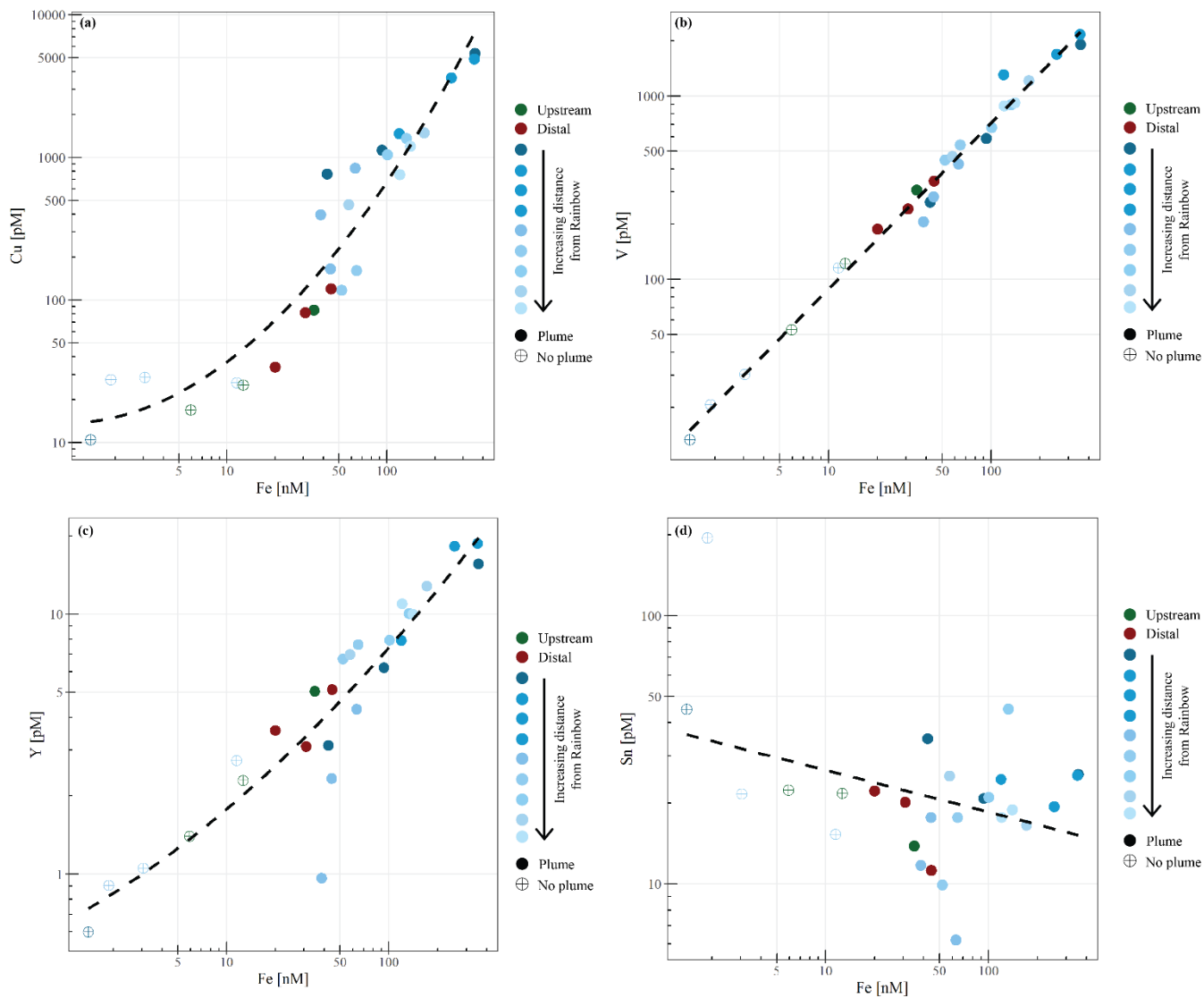
856 *Figure 4: (a) NMDS ordination showing all water samples based on their resemblance in chemical composition.*  
 857 *(b) NMDS ordination showing all plume samples from the downstream stations based on their resemblance in*  
 858 *chemical composition.*



859

860 *Figure 5: Relationship between in-situ measured turbidity and molar concentration of particulate iron.*

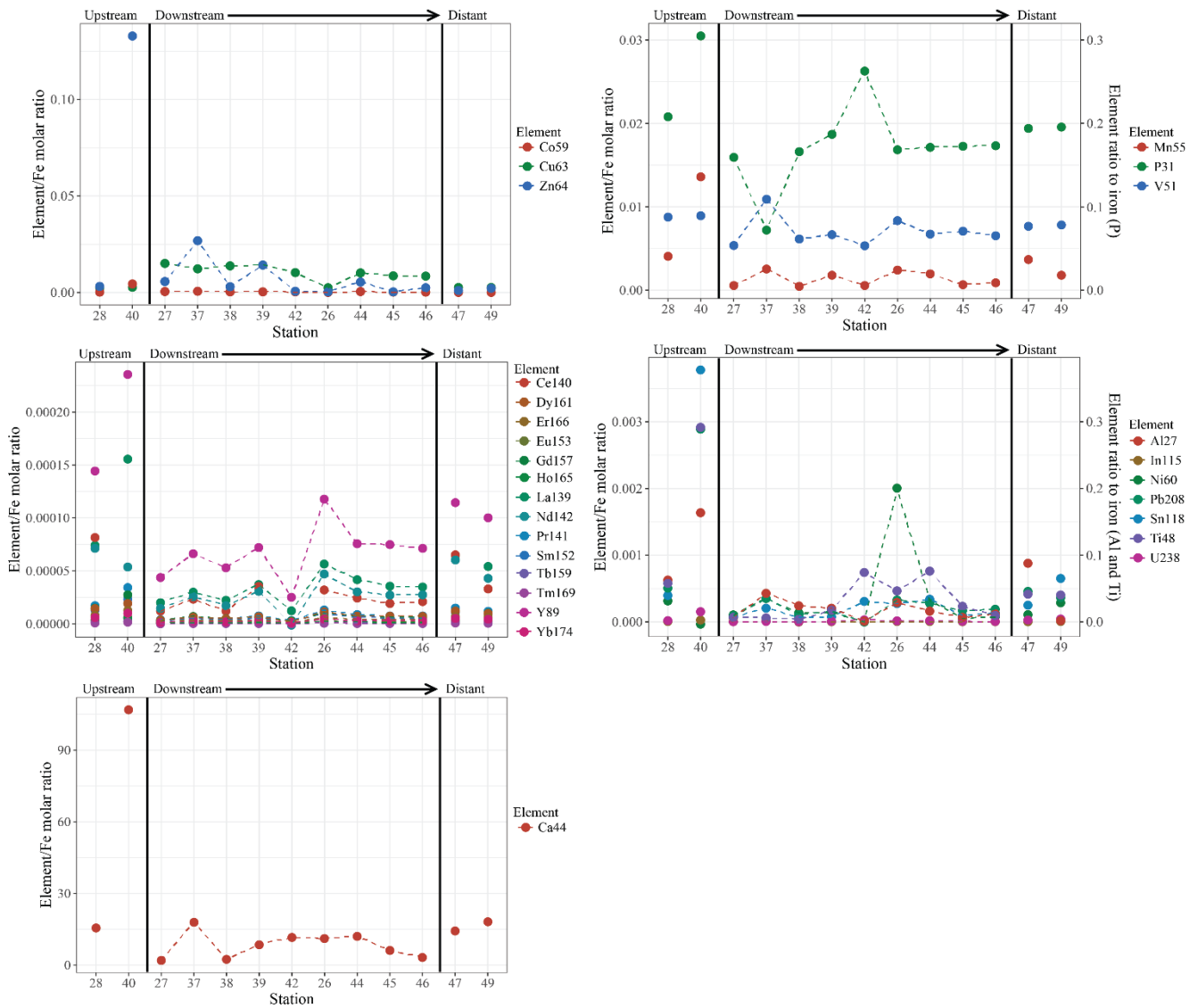
861



862

863 *Figure 6: Relationships between molar concentrations of particulate copper (a), vanadium (b), yttrium (c) and*  
 864 *tin (d) to iron.*

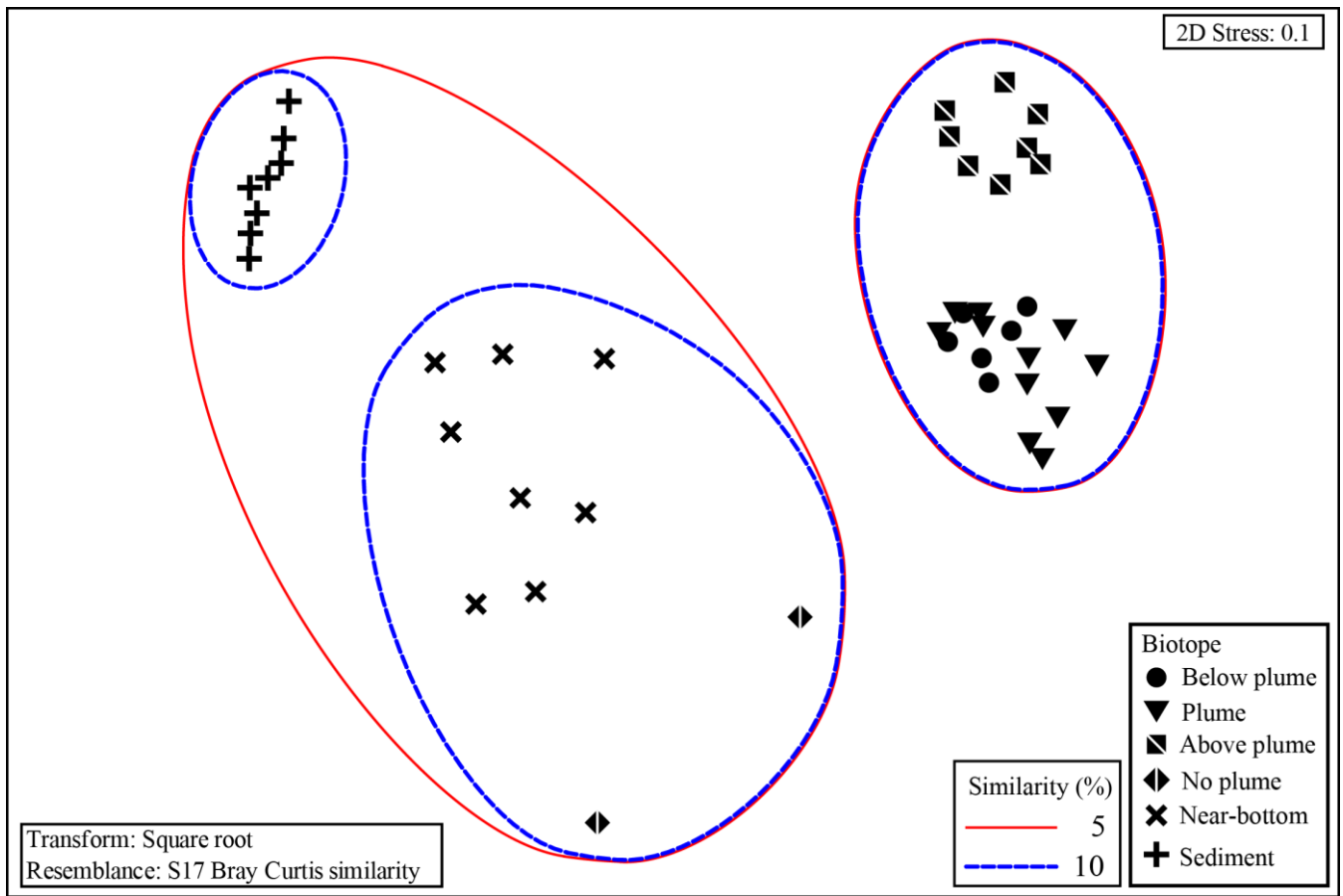
865



866

867 *Figure 7: Element to iron molar ratios. Plume samples of upstream, downstream and distant stations. Downstream*  
 868 *stations follow the main path of the plume. Fig. 7a) shows the element/Fe molar ratios of the chalcophiles (Co, Cu*  
 869 *and Zn), b) shows the ratios of Mn and the oxyanions (P and V), c) displays the ratios of REE, d) the ratios of Al,*  
 870 *In, Ni, Pb, Sn, Ti and U and e) shows the Ca/Fe molar ratio.*

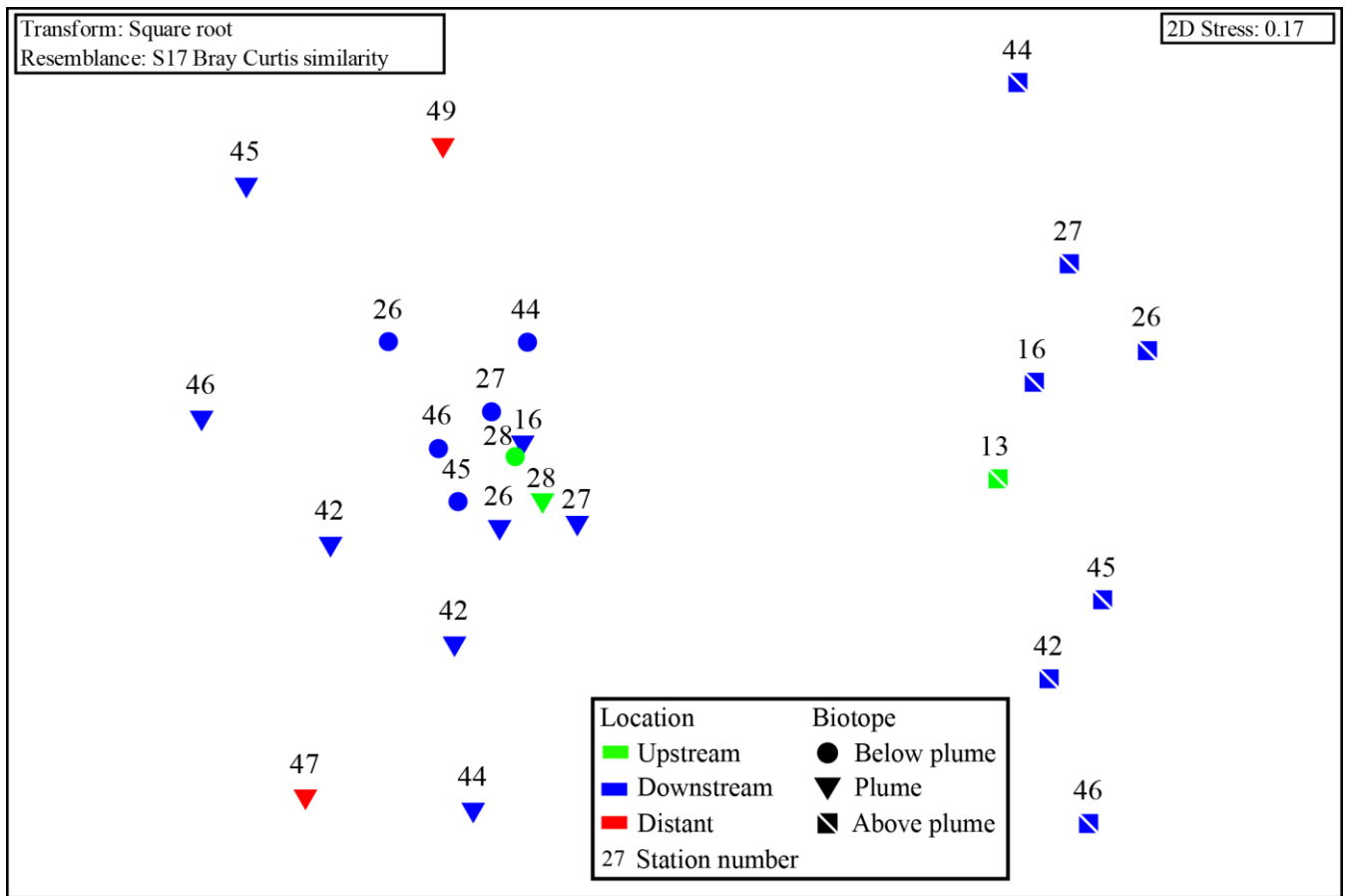
871



872

873 *Figure 8: Non-metric multidimensional scaling plot of the microbial community composition of all samples based*  
 874 *on Operational Taxonomic units. Similarity groupings are based on group average clustering. "No plume" is*  
 875 *representative of samples collected from station 13, where there was no indication of a plume.*

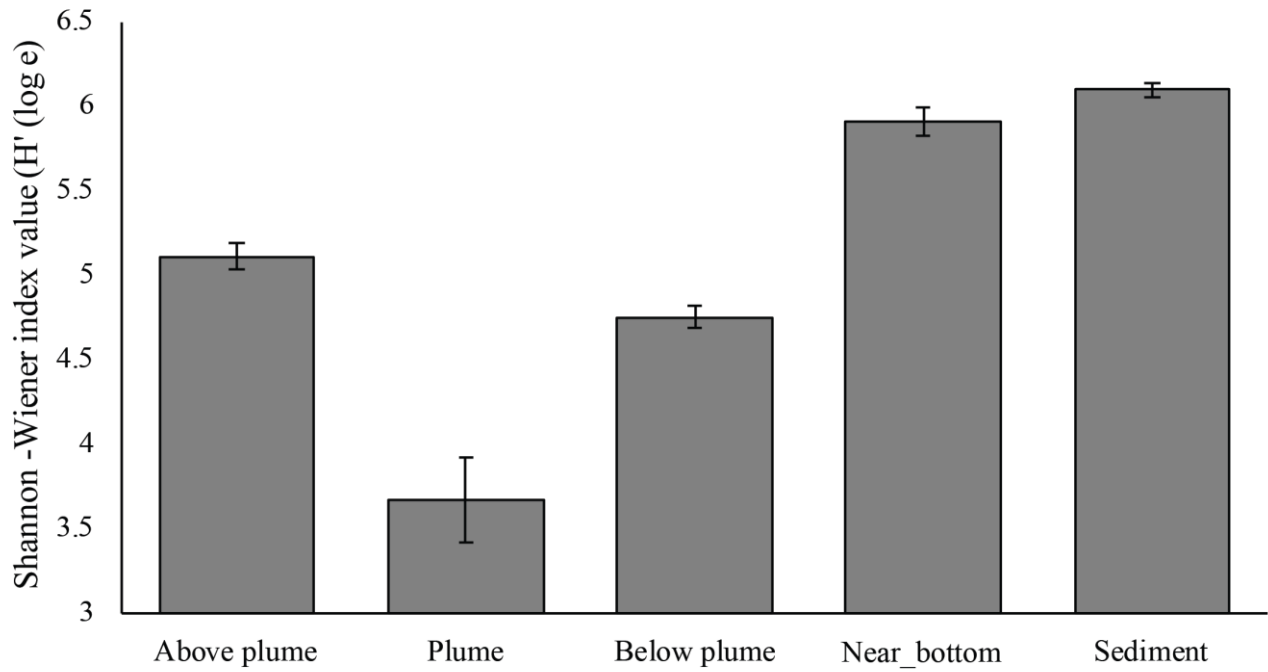
876



877

878 *Figure 9: Non-metric multidimensional scaling plot of the microbial community composition of all water column*  
 879 *samples based on Operational Taxonomic units. Plume and below plume depths from Station 13 were excluded.*

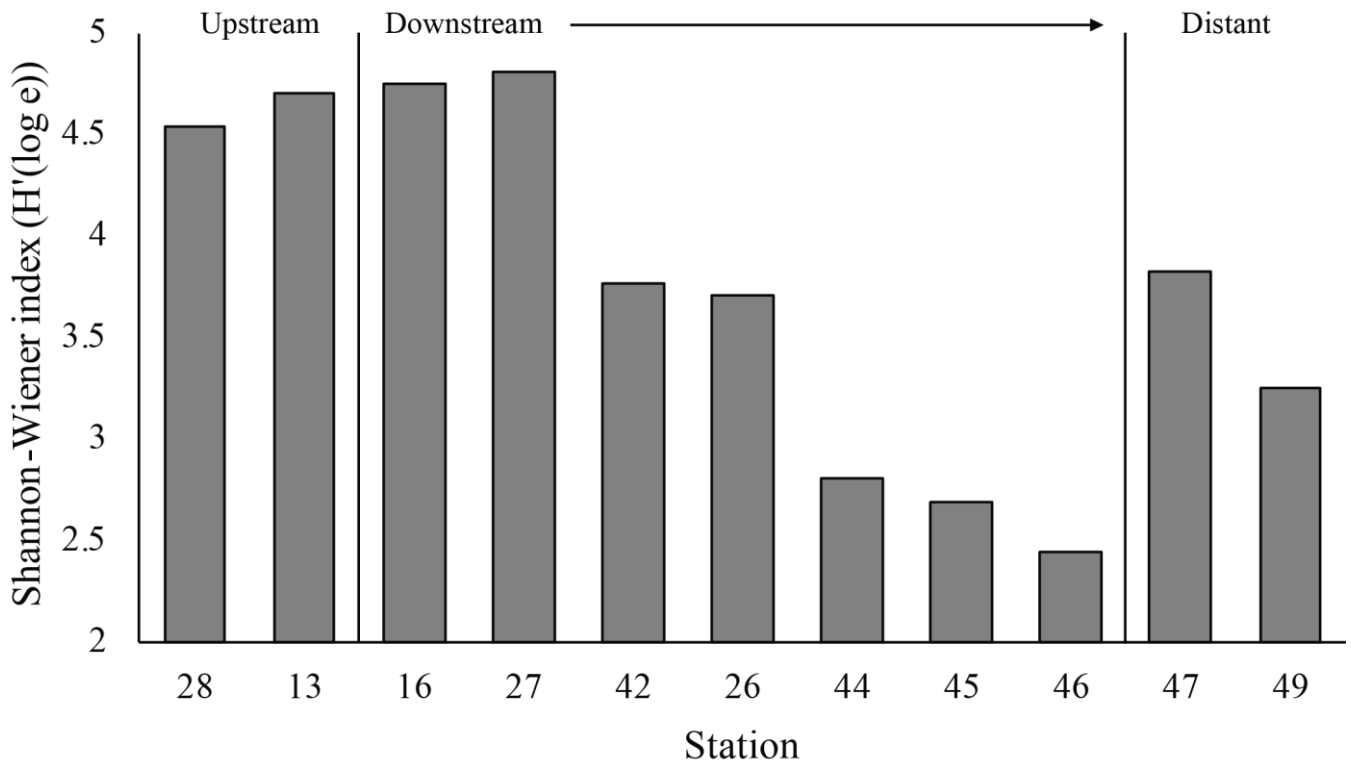
880



881

882 *Figure 10: Mean Shannon-Wiener diversity index for microorganisms in each biotope. Error bars represent ±SE*

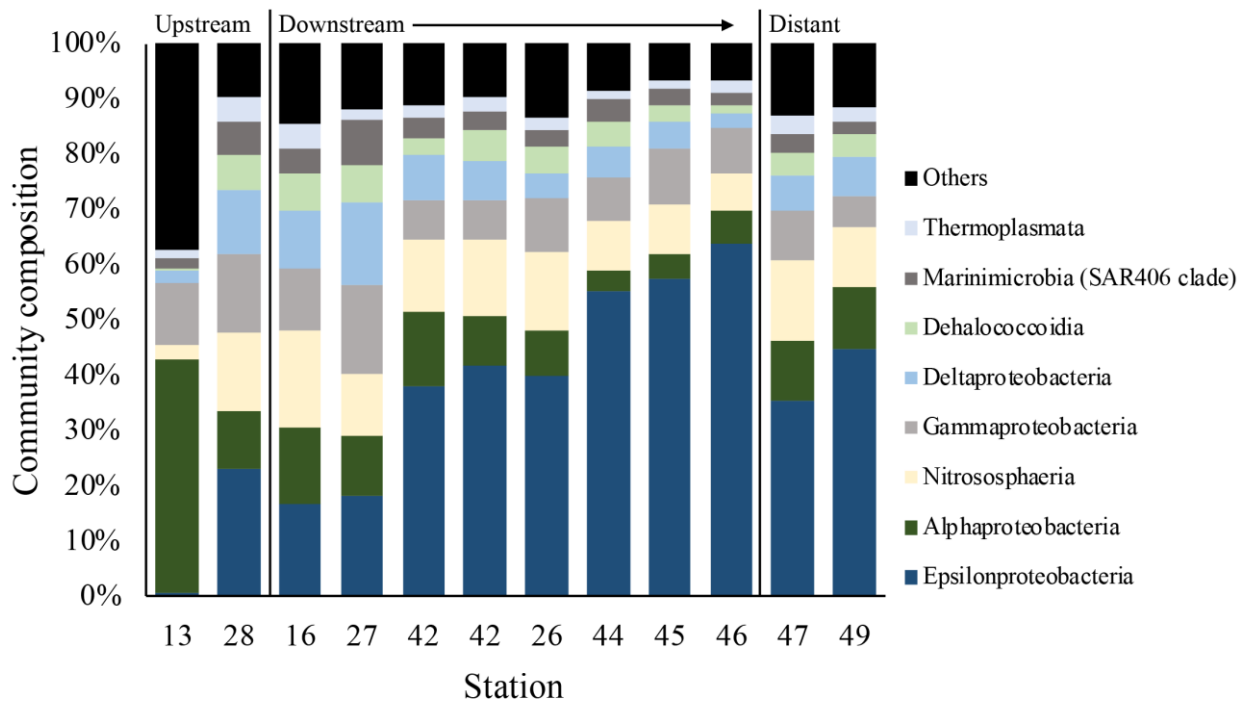
883



884

885 *Figure 11: Shannon-Wiener index values for microorganisms in each plume sample taken.*

886



887

888 *Figure 12: Microbial community composition in the plume samples as a percentage of the dominant class groups*  
 889 *in accordance with the SIMPER results.*

890

Station	Latitude	Longitude	Biotope	Sample type	Depth (m)	Microbiology	SPM	(Trace) metals
30	36°13'19"N	33°52'46"W	Sediment and near-bottom water	Box core	1970	x		
31	36°13'47"N	33°57'00"W	Sediment and near-bottom water	Box core	3190	x		
33	36°14'51"N	33°52'41"W	Sediment and near-bottom water	Box core	2223	x		
36	36°16'13"N	33°51'06"W	Sediment and near-bottom water	Box core	2857	x		
50	36°13'47"N	33°47'60"W	Sediment and near-bottom water	Box core	3157	x		
54	36°11'57"N	33°53'46"W	Sediment and near-bottom water	Box core	2129	x		
56	36°13'21"N	33°51'31"W	Sediment and near-bottom water	Box core	2198	x		
58	36°13'21"N	33°50'31"W	Sediment and near-bottom water	Box core	2514	x		
13	36°12'35"N	33°56'31"W	Above plume	CTD	125	x		
13	36°12'35"N	33°56'31"W	Below plume	CTD	3220	x		
13	36°12'35"N	33°56'31"W	Plume	CTD	2000	x		
16	36°14'10"N	33°53'37"W	Plume	CTD	1944	x		
16	36°14'10"N	33°53'37"W	Above plume	CTD	998	x		
26	36°16'41"N	33°50'29"W	Below plume	CTD	2756	x	x	x
26	36°16'41"N	33°50'29"W	Plume	CTD	2150	x	x	x
26	36°16'41"N	33°50'29"W	Plume	CTD	2000		x	x
26	36°16'41"N	33°50'29"W	Above plume	CTD	999	x	x	x
27	36°16'52"N	33°52'45"W	Below plume	CTD	2191	x		x
27	36°16'52"N	33°52'45"W	Plume	CTD	2077	x		x
27	36°16'52"N	33°52'45"W	Plume	CTD	1996			x
27	36°16'52"N	33°52'45"W	Above plume	CTD	994	x		x
28	36°10'54"N	33°57'40"W	Below plume	CTD	3170	x	x	x
28	36°10'54"N	33°57'40"W	Plume	CTD	1975	x	x	x
32	36°14'55"N	33°52'46"W	Plume	CTD	2192		x	
32	36°14'55"N	33°52'46"W	Plume	CTD	2088		x	
37	36°15'11"N	33°52'19"W	Plume	CTD	2190			x
38	36°15'11"N	33°52'17"W	Plume	CTD	2040			x
39	36°15'13"N	33°52'17"W	Plume	CTD	2019			x
40	36°11'57"N	33°53'18"W	No plume	CTD	2120			x
42	36°15'45"N	33°51'54"W	Plume	CTD	2291	x	x	x
42	36°15'45"N	33°51'54"W	Plume	CTD	2209	x	x	x
42	36°15'45"N	33°51'54"W	Plume	CTD	2037		x	x
42	36°15'45"N	33°51'54"W	Above plume	CTD	999	x	x	x
44	36°13'47"N	33°49'59"W	Below plume	CTD	2623	x		
44	36°13'47"N	33°49'59"W	Plume	CTD	2202		x	x
44	36°13'47"N	33°49'59"W	Plume	CTD	2002	x	x	x
44	36°13'47"N	33°49'59"W	Above plume	CTD	995	x		
45	36°13'46"N	33°46'33"W	Below plume	CTD	3004	x		
45	36°13'46"N	33°46'33"W	Plume	CTD	2166		x	x
45	36°13'46"N	33°46'33"W	Plume	CTD	2002	x	x	x
45	36°13'46"N	33°46'33"W	Above plume	CTD	996	x		
46	36°13'49"N	33°43'59"W	Below plume	CTD	2622	x		
46	36°13'49"N	33°43'59"W	Plume	CTD	2280	x	x	x
46	36°13'49"N	33°43'59"W	Plume	CTD	2145		x	x
46	36°13'49"N	33°43'59"W	Above plume	CTD	1000	x		
47	36°19'06"N	33°47'36"W	Below plume	CTD	2850			
47	36°19'06"N	33°47'36"W	Plume	CTD	2200	x		x
49	36°22'19"N	33°51'31"W	Plume	CTD	2260	x	x	x
49	36°22'19"N	33°51'31"W	Plume	CTD	1902		x	x

893 *Table 2: Primers used for sequencing.*

Forward		Reverse		Ratio in mix	Reference
Primer name	Primer sequence 5'-3'	Primer name	Primer sequence 5'-3'		
Arch-0519-a-S-1 (universal)	CAGCMGCCGCGGTAA	Bact-0785-b-A-18  (universal)	TACNVGGGTATCTAATCC	3/9 + 3/9	Klindworth et al. 2012
Bact-0519F  (targets WS6, TM7, OP11)	CAGCAGCATCGGTVA			1/9	This paper
Nano-0519F  (targets Nanoarchaea)	CAGTCGCCRCGGGAA	Nano-0785R  (targets Nanoarchaea)	TACNVGGGTMTCTAATYY	1/9+1/9	This paper

894

895

896 Table 3: SIMPER similarity results of each biotope at class level. \*\* undefined class.

Biotope	Average similarity (%)	Class	Average proportion (%)	Average similarity	Sim/SD	Contribution (%)	Cumulative %
Above plume	82.34	Nitrososphaeria	27.10	22.79	4.61	27.67	27.67
		Alphaproteobacteria	18.34	15.22	4.15	18.49	46.16
		Gammaproteobacteria	13.44	11.58	5.52	14.07	60.23
		Deltaproteobacteria	10.67	8.46	3.38	10.27	70.50
		Marinimicrobia (SAR406 clade)	8.22	6.96	6.07	8.46	78.96
		Dehalococcidia	6.38	5.69	9.19	6.91	85.87
		Thermoplasmata	2.63	2.26	5.68	2.74	88.61
		Acidimicrobiia	2.13	1.89	8.62	2.30	90.91
Plume	76.74	Epsilonproteobacteria	39.59	30.29	2.53	39.47	39.47
		Nitrososphaeria	12.16	10.32	4.05	13.45	52.92
		Gammaproteobacteria	9.69	7.92	4.71	10.32	63.23
		Alphaproteobacteria	9.23	7.22	2.44	9.40	72.64
		Deltaproteobacteria	7.60	5.56	2.75	7.25	79.88
		Dehalococcidia	4.57	3.55	2.58	4.63	84.51
		Marinimicrobia (SAR406 clade)	4.02	3.07	3.83	4.00	88.51
		Thermoplasmata	2.56	1.94	3.39	2.53	91.04
Below plume	77.94	Nitrososphaeria	22.35	16.60	3.29	21.30	21.30
		Alphaproteobacteria	13.26	11.43	5.18	14.67	35.97
		Deltaproteobacteria	10.88	9.25	8.31	11.87	47.84
		Gammaproteobacteria	10.60	8.89	7.78	11.40	59.24
		Epsilonproteobacteria	9.65	7.18	2.50	9.22	68.46
		Dehalococcidia	7.84	6.97	7.89	8.95	77.40
		Marinimicrobia (SAR406)	6.32	4.49	2.31	5.76	83.16
		Thermoplasmata	4.69	3.04	2.20	3.90	87.07
		Phycisphaerae	1.97	1.75	7.60	2.24	89.31
		Planctomycetacia	2.03	1.50	2.96	1.93	91.23
		Near-bottom water	75.71	Gammaproteobacteria	20.79	16.77	3.18
Nitrososphaeria	16.90			13.54	3.79	17.89	40.04
Alphaproteobacteria	15.55			13.25	5.47	17.50	57.54
Deltaproteobacteria	6.68			5.89	5.99	7.78	65.32
Oxyphotobacteria	5.93			4.04	2.18	5.34	70.66
Dehalococcidia	4.08			2.99	2.50	3.95	74.61
Phycisphaerae	3.72			2.57	2.03	3.40	78.01
Thermoplasmata	2.47			1.70	2.25	2.24	80.25
Acidimicrobiia	2.06			1.61	2.72	2.13	82.38
Bacteroidia	2.15			1.57	1.85	2.07	84.45
Marinimicrobia (SAR406 clade)	1.75			1.24	2.17	1.64	86.09
OM190	1.64			1.14	2.02	1.51	87.60
Planctomycetacia	1.40			1.09	2.76	1.44	89.04
Epsilonproteobacteria	1.71			0.85	1.08	1.12	90.16
Sediment	82.51			Gammaproteobacteria	29.67	27.17	8.51
		Alphaproteobacteria	13.98	12.44	4.88	15.07	48.01
		Deltaproteobacteria	11.98	10.98	10.24	13.30	61.31
		Nitrososphaeria	7.73	5.69	3.74	6.90	68.21
		Phycisphaerae	5.46	5.01	7.85	6.07	74.28
		Dehalococcidia	3.35	2.48	2.58	3.01	77.29
		BD2-11 terrestrial group	2.36	1.91	2.90	2.31	79.60
		Subgroup 22 (Acidobacteria)	2.10	1.74	3.22	2.11	81.71
		OM190	2.09	1.50	5.50	1.81	83.53
		Nitrospira	1.79	1.49	3.68	1.80	85.33
		Bacteroidia	1.91	1.48	3.66	1.79	87.12
		Acidimicrobiia	1.58	1.24	2.84	1.50	88.62
		Thermoanaerobaculia	1.41	1.07	3.25	1.30	89.92
		Gemmatimonadetes**	1.57	1.06	1.56	1.28	91.21